Complex Embedded Automotive Control Systems
CEmACS

DaimlerChrysler
SINTEF
Glasgow University
Hamilton Institute
Lund University

Vehicle state observer requirement specification

Public
Interrim Report Work Package 4
Deliverable D10

September 2005

Contents

Executive Summary

This requirement specification report describes the requirements imposed on vehicle state observers based on work carried out up to month 12 in Work Package 4 of the CEMACS project (deliverable D10).

The main objective of the specification document is to support the design and implementation of a nonlinear observer for vehicle velocity and other variables. These observers are of interest as stand-alone modules as one of the objectives of the project is to evaluate the possibility of design of nonlinear observers with theoretical convergence properties, at least as good performance as the Extended Kalman Filters, and with less real-time computational complexity and simplified tuning. Moreover, these observers will be used to provide state estimates for controllers developed in Work Packages 1 and 2 of this project.

The scope of work in Work Package 4 is limited to specification, design, implementation and validation of observers at a prototype level to demonstrate their usefulness and estimate limitations of performance.

Chapter 1

Introduction

1.1 Background and motivation

Complex automotive control systems rely heavily on accurate and reliable information about the state of the vehicle and its environment. While certain state variables, such as yaw rate, are measured directly, others, such as the vehicle's side slip angle, cannot be measured due to high sensor costs. The use of model-based state estimators is therefore necessary to provide estimates of unmeasured states and achieve sensor fusion when there are redundant or distributed sensors. In addition, it provides a mechanism to achieve safe and graceful degradation of performance when there is temporary or permanent errors in some of the vehicle sensors.

With the vehicle dynamics being nonlinear, observability will depend on state and inputs of the system. As a matter of fact external disturbances such as the friction coefficient between tyre and road or the inclination of the road are only conditionally observable, depending on the driving situation.

Recently, there has been significant progress in the design of nonlinear observers, which provides an attractive alternative to the Extended Kalman-Filter (EKF) due to such properties as simplicity of implementation and tuning, and reduced on-board computational complexity.

Beyond these technological advantages, an important point is that there exist several methods and principles for the proof of uniform global or regional asymptotical/exponential stability for the non-linear observer error dynamics, including nonlinear dissipative forces such as friction and bias models (e.g. due to sensor drift). These theoretical issues are becoming increasingly important from a practical engineer's point of view since in complex safety-critical automotive control systems a theoretical foundation is likely to avoid design errors and reduce the time used for tuning, verification and testing.

We conclude that the potential advantages of using nonlinear observers in automotive applications are significant. Moreover, a combination of EKF and nonlinear observers can solve the global convergence problem while maintaining the benefits of tuning and monitoring local performance in a well established way.

1.2 Scope of work

The main objective of the specification document is to support the design and implementation of a nonlinear observer for vehicle velocity and other variables. These observers are of interest as stand-alone modules as one of the objectives of the project is to evaluate the possibility of design of nonlinear observers with theoretical convergence properties, at least as good performance as the Extended Kalman Filters, and with less real-time computational complexity and simplified tuning. Moreover, these observers will be used to provide state estimates for controllers developed in Work Packages 1 and 2 of this project.

The scope of work is limited to specification, design, implementation and validation of observers at a prototype level to demonstrate their usefulness and estimate limitations of performance.

Chapter 2

Vehicle Velocity Observer Requirement Specification

2.1 Vehicle dynamics and kinematics

The horizontal plane and vertical motion states and parameters of the four-wheeled vehicle are illustrated in Figures 2.1 and 2.2, respectively. The wheel states and parameters are illustrated in Figure 2.3.

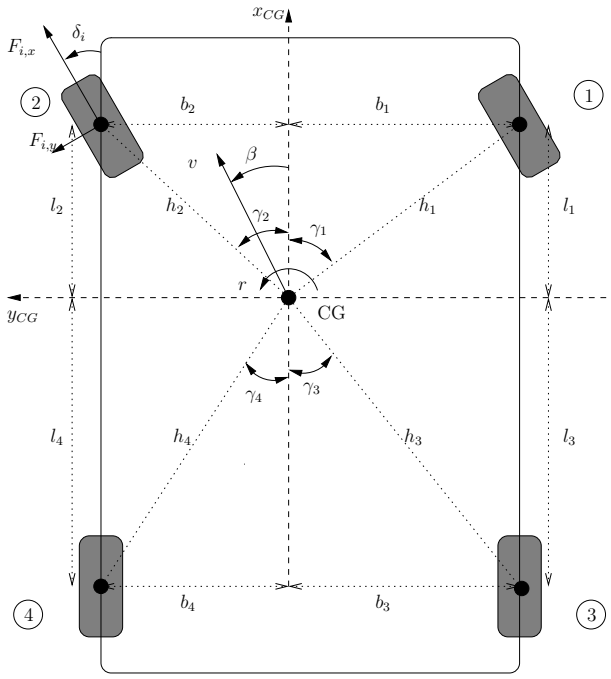

Figure 2.1: Horizontal plane motion variables and parameters of the vehicle

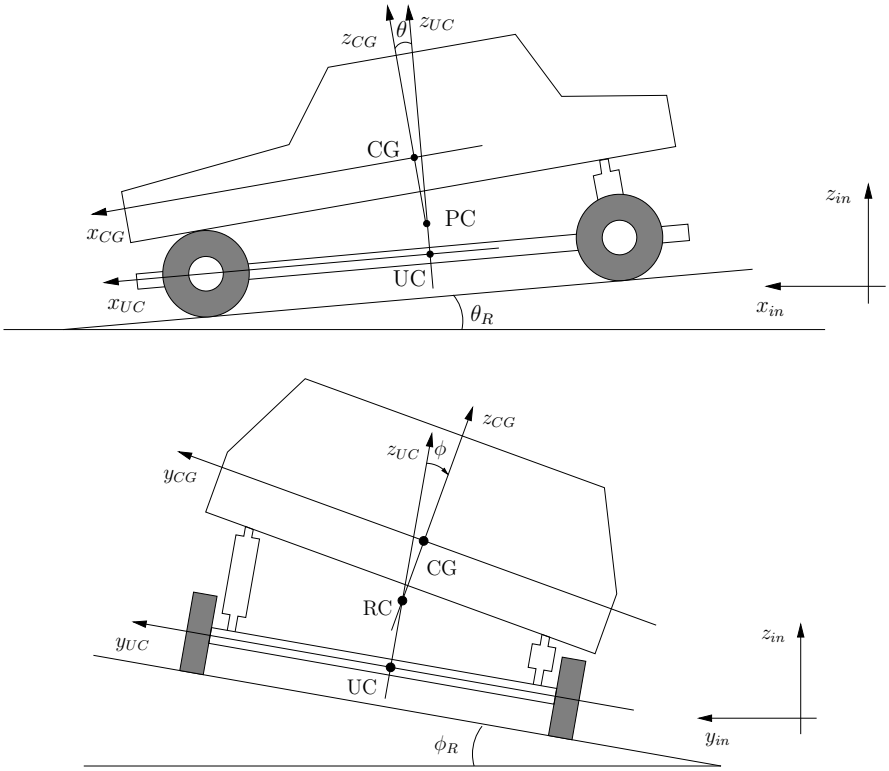

Figure 2.2: Vertical motion variables and parameters of the vehicle

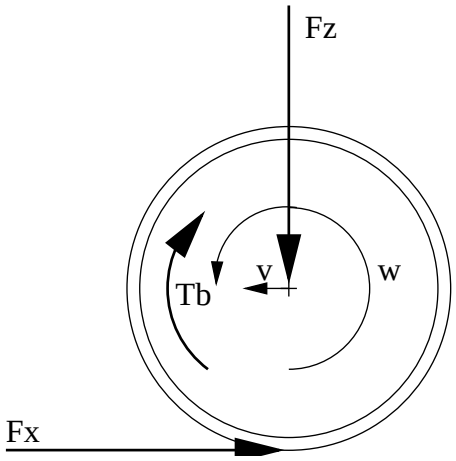

Figure 2.3: Wheel variables and parameters of the vehicle

2.2 Functional requirements

The vehicle velocity observer will be used both for the integrated chassis control (generic prototype, Work package 2) and for collision avoidance (active safety, Work package 1). Although the primary states to be estimated are the same for these two applications, the secondary states necessary (as well as performance requirements) will differ.

Additionally, the velocity observer should be suited for dynamic vehicle handling systems such as ESP.

2.2.1 States to be estimated

The primary states to be estimated are

- Lateral velocity of vehicle, v_x.
- Longitudinal velocity of vehicle, v_y.

The following secondary states are expected to be necessary to estimate in order to achieve necessary accuracy of the internal nonlinear model in the observer

- Yaw rate, r.
- Road-tyre adhesion coefficient (maximum friction coefficient), μ_H, or possibly other parameter(s) of the friction model.

Including a friction coefficient estimate is not essential for the generic prototype (Work package 2) as the prototype can be assumed to be driving at high friction roads. Furthermore, the following states may be necessary to estimate to achieve required accuracy for collision avoidance application in Work package 1:

- Road bank angle, ϕ_R.
- Position of vehicle center of gravity (x_{CG}, y_{CG}, z_{CG}).

2.2.2 Operating modes

The state observer is required to provide reliable state estimates in the *normal operating mode*, i.e. all driving maneuvers with positive longitudinal velocity, $v_x > 0$, and side slip angle β absolute value less than 90 degrees.

The state observer should be able to execute during all other operating conditions, including stand-still and reverse driving. If reliable estimates are not provided under such conditions, the observer is required to provide a quality indicator flag and is also required to immediately provide reliable estimates once the normal operating mode is entered.

2.2.3 Robustness to road, tyres, load and environmental conditions

The generic prototype will experience rather small parameter variations (friction, tyres and load). The following applies therefore foremost to the collision avoidance application (see also performance requirements):

- The state observer must provide reliable estimates under a wide range of road and environmental conditions ranging from wet ice to dry asphalt.
- The behavior of the observer should be robust to tyre brand, wear and tear of tyre, and normal variations in tyre pressure.
- The observer should be robust towards permissable variations in load and mass distribution.

2.2.4 Sensor configurations and data input requirements

The assumed sensor configuration corresponds to a basic car with an ABS system and ESP sensors

- Wheel speed or wheel position
- Steering angle (for all four wheels for generic prototype)
- Longitudinal accelerometer
- Lateral accelerometer
- Yaw rate

In addition, for some vehicles the following may be available

- Brake pressures (giving an indication of brake torque) (only in experimental cars)
- Engine speed (in production cars)
- Engine torque (both static and dynamic, includes other loads)
- ESP flag
- Brake Assist flag (not in test cars)
- ABS flag for each wheel (for test cars: with μ_H estimate for each wheel)
- Stand still flag

For a detailed description of the instrumentation of the test vehicles, it is referred to the project report D11 [2].

2.2.5 Fault tolerance and graceful degradation

Failures of yaw rate, wheel speed / position sensors are not to be considered, nor is detection of such sensor failure.

The robust performance of the nonlinear observers subject to partial or complete failure of the following sensors should be evaluated:

- Steering angle
- Longitudinal and lateral acceleration

Single point failure handling strategies such as replacing faulty sensor signals with nominal or calculated values should be tested. The performance of the nonlinear observer should degrade gracefully when sensors fail.

Accelerometer signals are assumed to drift slowly, while wheel speed / position, yaw rate and steering angle signals are not assumed to drift or have significant bias.

The sensitivity of the observer with respect to sensor location (in particular accelerometers) should be evaluated as the center of gravity will change with the vehicle load conditions.

2.3 Performance requirements

2.3.1 Model requirements

The vehicle model used in the observer should account for the following physical effects

- Nonlinear equations of motion in the horizontal plane (lateral, longitudinal and yaw motion).
- Coriolis effect
- Nonlinear lateral and longitudinal slip dependent road-tyre friction forces
- Vehicle mass distribution and inertia
- The gross effect of vehicle roll and pitch motion should be accounted for using accelerometer signals

2.3.2 Estimator accuracy

- For the generic prototype, stationary error in side slip should normally be less than 0.1°.
- For collision avoidance, side slip error should normally be less than 1°.

2.3.3 Estimator bandwidth

The time delay introduced by the filter should not be larger than 20 ms for the velocity estimates. The response time should match the DaimlerChrysler Extended Kalman Filter. If these requirements hold, the estimator bandwidth is well over what is required for integrated chassis control and collision avoidance.

There are no accuracy or bandwidth requirements on the other variables, such as adhesion coefficient estimate.

2.4 Parameterization

2.4.1 Model parameterization requirements

Etimates of the following model tuning parameters are assumed to be available:

- Vehicle mass
- Location of center of gravity (CG)
- Moment of inertia about vertical axis
- Suspension stiffness coefficient in roll and pitch
- Location of wheels with respect to CG
- Dynamic wheel radius
- Tyre friction characteristic (analytical model or lookup table, depending on lateral and longitudinal slips and adhesion coefficient).

2.4.2 Observer tuning requirements

The observer should contain as few tuning parameters (gains) as possible, and the tuning parameters should as far as possible be chosen to scale with key vehicle parameters such as mass.

2.5 Implementation requirements

2.5.1 Real-time constraints

The observer must be possible to implement on standard electronic control units at a sampling rate of 100 Hz. CPU and memory requirements should be significantly less than an Extended Kalman Filter.

2.5.2 Software prototype platform

Prototype observers should be implemented in Simulink release 13. This will ensure compatibility with the Real time workshop code generation tools for the dSpace system installed in DaimlerChrysler's experimental vehicles, [2].

2.6 Verification and validation requirements

2.6.1 Comparison with EKF

The nonlinear observer implementation should be compared in detail with the Extended Kalman Filter developed by DaimlerChrysler. The following aspects should be considered

- Accuracy (bandwidth, noise sensitivity, bias) under test maneuvers.
- Computational complexity (number of arithmetic operations or clock cycles per sample) and real-time memory usage.
- Simplicity of tuning
- Robustness and reliability under all conditions

2.6.2 Test maneuvers

- For the generic prototype application, the observer will be tested at least using the following test maneuvers on high friction surfaces:
  - Straight ahead driving with increasing and decreasing speed
  - Slalom maneuvers
  - Driving in circle while increasing speed
- For the collision avoidance application, the observer will be tested using the same test maneuvers, in addition to driving in circle on tilted ground. Also, some of the maneuvers will be tested on low friction surfaces.

2.6.3 Verification and validation

- Off-line experimental validation using test data.

Filename	Comment
743SL507.SAM	Slalom maneuver, high friction
743SL510.SAM	Slalom maneuver, high friction
743SK101.SAM	Driving in circle, high friction
743SK104.SAM	Driving in circle, high friction
743SK402.SAM	Driving in circle, low friction
743SK204.SAM	Driving in circle, low friction
220ALP13.SAM	Hilly roads, high friction
220ALP19.SAM	Hilly roads, high friction

- In-vehicle testing according to the test plans of Work packages 1 and 2.

Chapter 3

Preliminary velocity observer design, no friction estimation

This chapter is based on the paper [7].

Abstract

Nonlinear observers for estimation of lateral and longitudinal velocity of automotive vehicles are proposed, based on acceleration and yaw rate measurements in addition to wheel speed and steering angle measurements. Two approaches are considered, one modular approach where the estimated longitudinal velocity is used as input to an observer for lateral velocity. The second approach is a combined approach where all states are estimated in the same observer. In both approaches, a tyre-road friction model is used for estimation of lateral velocity. Stability of the observers are proved in the form of input-to-state stability of the observer error dynamics, under a structural assumption on the friction model. This assumption is treated with some detail. The observers are validated on experimental data from cars.

3.1 Introduction

Feedback control systems for active safety in automotive applications have over the last years entered production cars. Many of these systems (for instance yaw stabilization systems such as ESP [24]) have in common that the control action depend on information about vehicle velocity, or side-slip. However, the velocity is seldom measured directly, and must therefore be inferred from other measurements such as wheel speed, yaw rate, and acceleration measurements.

The main goal of this work is to develop nonlinear observers for vehicle velocity with stability guarantees. Towards this goal, we propose two nonlinear observer structures: First a modular cascaded observer structure where the estimation of lateral and longitudinal velocity is separated, and thereafter a combined observer for both velocities. We establish input-to-state stability (ISS) of both observer structures, under a realistic condition on the friction model.

Nonlinear observers are used for taking the nonlinear dynamics (mainly due to highly non-linear friction and Coriolis forces) into account, and to obtain simple designs with few tuning knobs (as opposed to Extended Kalman Filter designs). Another significant advantage of the proposed approach is that real-time solution of the Riccati differential equations is avoided, such that the observer can be implemented more efficiently in a low-cost embedded computer unit.

A non-linear friction model is used for exploiting the lateral acceleration measurement in full. An important parameter in many friction models, the maximal friction coefficient μ_H, is known to vary significantly with different road conditions. We will assume this parameter to be known, or estimated by other means. While simultaneous estimation of velocity and μ_H might be a feasible path, we argue that estimation of μ_H requires special attention depending on the application the observer is used for, since it will be only weakly observable for many (normal) driving conditions, requiring monitoring, resetting and other logic functions to be implemented (see e.g. [10]).

Earlier works on observers for estimation of lateral velocity are mainly based on linear or quasi-linear techniques, e.g. [4, 25, 23, 3]. A nonlinear observer linearizing the observer error dynamics have been proposed in [12, 13]. The same type of observer, in addition to an observer based on forcing the dynamics of the nonlinear estimation error to the dynamics of a linear reference system, are investigated in [6]. The problem formulation there assumes that the longitudinal wheel forces are known, as the observer implemented in ESP also does [24]. In our work, we do not make this assumption, as such information is not always available. Nevertheless, if this information *is* available, it might be natural to use it in the first module of our modular approach (estimation of longitudinal velocity).

The Extended Kalman Filter (EKF) is used for estimating vehicle velocity and tyre forces in [19, 20], thus without the explicit use of friction models. A similar, but simpler, approach is suggested in [3]. An EKF based on a tyre-road friction models that also included estimation of the adhesion coefficient and road inclination angle is suggested in [22]. In [1], the use of an EKF is considered, based on a nonlinear tyre-friction model, that also includes estimation of cornering stiffness. The strategy proposed in [15] combines dynamic and kinematic models of the vehicle with numerical bandlimited integration of the equations to provide a side-slip estimate. In [5] the side-slip angle is estimated along with yaw rate in an approach that has similarities with the one considered herein, but without yaw-rate measurements. The approach is validated using experimental data, but there are no stability proofs.

A unique feature of our work presented here, is that explicit stability conditions are analyzed.

3.2 Vehicle modeling

3.2.1 Rigid body dynamics

The geometry of the vehicle and the coordinate systems are illustrated in Figure 3.1. The vehicle velocity is defined in a body-fixed coordinate system with the origin at the vehicle center of gravity (CG, assumed constant), with x-axis pointing forward

and y-axis to the left. There is also a coordinate system in the center of each wheel, aligned with the orientation of the wheel. The distance from CG to each wheel center is denoted h_i, with i being wheel index. Together with the angles γ_i, this defines the vehicle geometry.

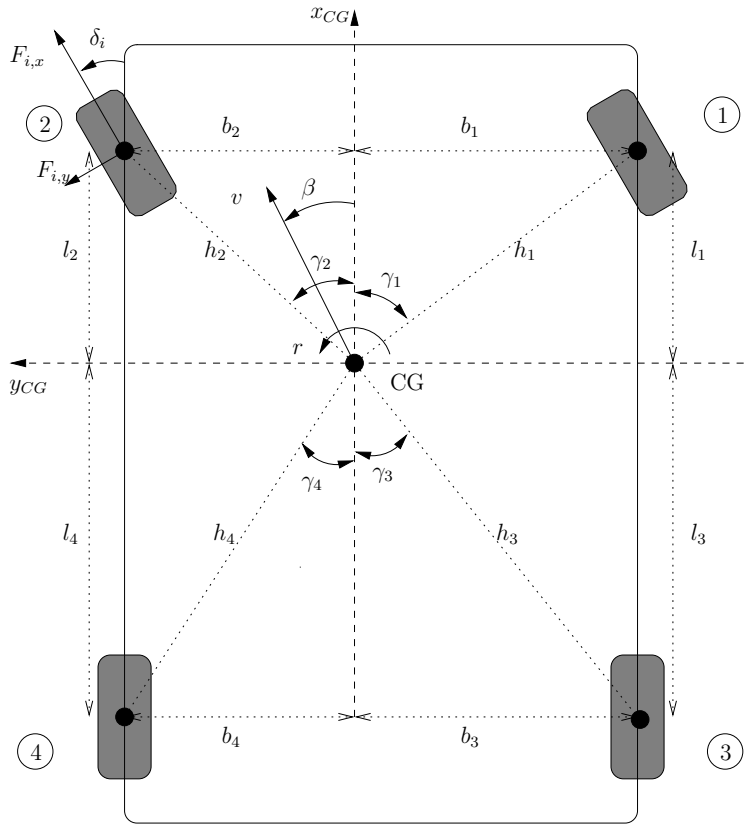

Figure 3.1: Horizontal axis systems, geometric definitions, wheel forces, speed, slip angle and yaw rate.

Neglecting suspension dynamics, we will assume that we can consider the vehicle a rigid body, for which the rigid body dynamics (with respect to the CG coordinate system) can be written

$$\mathbf{M}\dot{\nu} + \mathbf{C}(\nu)\nu = \tau \tag{3.1}$$

where $\boldsymbol{\nu}$ is a vector containing the body generalized velocities. The matrices $\mathbf{M}$ and $\mathbf{C}$ are the inertia, and Coriolis and centripetal matrices, respectively. The vector $\boldsymbol{\tau}$ consists of forces and torques on the vehicle, mainly friction forces acting via the wheels, but also gravitational and aerodynamic (wind and air resistance) forces are at work.

By making the following assumptions,

- only include motion in the plane (ignore dynamics related to vertical motion, including roll and pitch),
- ignore effect of caster and camber,

- only include tyre friction forces,

the vehicle dynamics are described by longitudinal velocity v_x, lateral velocity v_y and yaw rate r, resulting in the "two-track model" [13], with

$$\mathbf{M} = \begin{pmatrix} m & 0 & 0 \\ 0 & m & 0 \\ 0 & 0 & J_z \end{pmatrix}, \quad \mathbf{C}(\boldsymbol{\nu}) = \begin{pmatrix} 0 & -mr & 0 \\ mr & 0 & 0 \\ 0 & 0 & 0 \end{pmatrix}.$$

The generalized forces $\boldsymbol{\tau} = (f_x, f_y, \tau_z)^\mathsf{T}$ are forces and torque generated by friction between the wheels and the ground,

$$\boldsymbol{\tau} = \sum_{i=1}^{4} \begin{pmatrix} \mathbf{I}_{2\times 2} \\ \mathbf{g}_i^\mathsf{T} \end{pmatrix} \mathbf{R}(\delta_i)\mathbf{F}_i.$$

The friction forces $\mathbf{F}_i$ working at each wheel (see Figure 3.1) are functions of velocity difference between vehicle and tyres, see the next section. They are transformed from the wheel coordinate systems to CG:

- The forces generated by the tyres in body-fixed coordinates for each wheel i, is:

  $$\mathbf{f}_i = (f_{i,x}, f_{i,y})^\mathsf{T} = \mathbf{R}(\delta_i)\mathbf{F}_i$$

  where $\mathbf{F}_i = (F_{i,x}, F_{i,y})$ are the forces acting on the wheel in the wheel-fixed coordinate system. The rotation matrix induced by the steering angle δ_i is

  $$\mathbf{R}(\delta_i) = \begin{pmatrix} \cos\delta_i & -\sin\delta_i \\ \sin\delta_i & \cos\delta_i \end{pmatrix}.$$

- For the torque, it is convenient to define the geometry vector

  $$\mathbf{g}_i = \begin{pmatrix} -h_i \sin\psi_i \\ h_i \cos\psi_i \end{pmatrix}$$

  where the angles ψ_i are introduced to get a uniform representation, $\psi_1 = -\gamma_1$, $\psi_2 = \gamma_2$, $\psi_3 = \pi + \gamma_3$ and $\psi_4 = \pi - \gamma_4$. The generated torque about the vertical axis through the CG is then for each wheel

  $$\tau_{i,z} = \mathbf{g}_i^\mathsf{T}\mathbf{f}_i.$$

3.2.2 Friction models

In most friction models, the friction forces are functions of tyre slips, $\mathbf{F}_i = \mathbf{F}_i(\lambda_{i,x}, \lambda_{i,y})$, where the slips $\lambda_{i,x}$ and $\lambda_{i,y}$ are measures of the relative difference in vehicle and tyre longitudinal and lateral velocity for wheel i. The definitions for tyre slips we will use herein, are

$$\lambda_{i,x} = \frac{\omega_i R_{dyn} - V_{i,x}}{V_{i,x}}, \quad \lambda_{i,y} = \sin\alpha_i,$$

where ω_i is the wheel angular velocity and R_{dyn} is the dynamic wheel radius, and the tyre slip angles are calculated as

$$\alpha_i = \delta_i - \arctan \frac{v_{i,y}}{v_{i,x}},$$

and $V_{i,x}$ is the velocity in x-direction in the wheel coordinate system,

$$V_{i,x} = \sqrt{v_{i,x}^2 + v_{i,y}^2} \cos \alpha_i.$$

The longitudinal and lateral velocities of the wheel center in the body-fixed coordinate system are $v_{i,x} = v_x \pm r b_i$ and $v_{i,y} = v_y \pm r b_i$. For the tyre slip angles to be well defined, we assume for convenience that there is no reverse motion,

Assumption 1 *$v_{i,x} > 0$ for $i = 1, \ldots, 4$.*

The tyre slips depend on the vehicle states and the time-varying, measured steering angles $\boldsymbol{\delta} = (\delta_1, \ldots, \delta_4)^\mathsf{T}$ and wheel angular speeds $\boldsymbol{\omega} = (\omega_1, \ldots, \omega_4)^\mathsf{T}$. We will therefore use the notations $\mathbf{F}_i = \mathbf{F}_i(\lambda_{i,x}, \lambda_{i,y}) = \mathbf{F}_i(v_x, v_y, r, \delta_i, \omega_i)$ interchangeably, depending on context.

We make the following assumption on the friction model:

Assumption 2 *There exist a positive constant c_1 and sets Δ, Ω and a convex set $X(\boldsymbol{\delta}, \boldsymbol{\omega})$, such that the friction model is continuously differentiable in $\boldsymbol{\chi} = (v_x, v_y, r)^\mathsf{T}$ with $\|\frac{\partial \mathbf{F}_i(\boldsymbol{\chi}, \delta_i, \omega_i)}{\partial \boldsymbol{\chi}}\|$ bounded for $\boldsymbol{\chi} \in X(\boldsymbol{\delta}, \boldsymbol{\omega})$, $\boldsymbol{\delta} \in \Delta$ and $\boldsymbol{\omega} \in \Omega$, and*

$$\sum_{i=1}^{4} \left(\frac{\partial F_{i,y}(\boldsymbol{\chi}, \delta_i, \omega_i)}{\partial v_y} \cos \delta_i + \frac{\partial F_{i,x}(\boldsymbol{\chi}, \delta_i, \omega_i)}{\partial v_y} \sin \delta_i \right) < -c_1, \tag{3.2}$$

for all $\boldsymbol{\delta} \in \Delta$, $\boldsymbol{\omega} \in \Omega$, and $\boldsymbol{\chi} \in X(\boldsymbol{\delta}, \boldsymbol{\omega})$.

The physical meaning of this assumption is discussed in Section 3.5.

Remark 1 The sets $X(\boldsymbol{\delta}, \boldsymbol{\omega})$ and Δ will depend on which friction model is used. For example, using linear friction models (see Section 3.5.1), X depends on $\boldsymbol{\delta}$ only:

$$\begin{aligned} \Delta &= \{\delta_i \ : \ |\delta_i| \leq \bar{\delta}, \ i = 1, \ldots, 4\}, \\ X(\boldsymbol{\delta}) &= \{\boldsymbol{\chi} = (v_x, v_y, r)^\mathsf{T} : |\alpha_i| \leq \bar{\alpha}, \ |r| \leq \bar{r}, v_x > \bar{r} b_i\}. \end{aligned}$$

Note that α_i depends on δ_i. □

The following result regarding the friction forces holds due to Assumption 2:

Lemma 1 *There exist positive constants c_i, $i = 1, \ldots, 6$ such that for all $\boldsymbol{\chi}, \hat{\boldsymbol{\chi}} \in X(\boldsymbol{\delta}, \boldsymbol{\omega})$, $\boldsymbol{\delta} \in \Delta$, $\boldsymbol{\omega} \in \Omega$, the following holds:*

$$\tilde{v}_y \sum_{i=1}^{4} [0\ 1]\, \mathbf{R}(\delta_i) \left(\mathbf{F}_i(\boldsymbol{\chi}, \delta_i, \omega_i) - \mathbf{F}_i(\hat{\boldsymbol{\chi}}, \delta_i, \omega_i)\right) \leq -c_1 \tilde{v}_y^2 + c_2 |\tilde{r}||\tilde{v}_y| + c_3 |\tilde{v}_x||\tilde{v}_y| \quad (3.3a)$$

$$\frac{1}{J_z} \sum_{i=1}^{4} \mathbf{g}_i^{\mathsf{T}} \mathbf{R}(\delta_i) \left(\mathbf{F}_i(\boldsymbol{\chi}, \delta_i, \omega_i) - \mathbf{F}_i(\hat{\boldsymbol{\chi}}, \delta_i, \omega_i)\right) \leq c_4 |\tilde{v}_y| + c_5 |\tilde{r}| + c_6 |\tilde{v}_x| \quad (3.3b)$$

where $(\tilde{v}_x, \tilde{v}_y, \tilde{r}) := \boldsymbol{\chi} - \hat{\boldsymbol{\chi}}$. □

PROOF If we let $h(\boldsymbol{\chi}, \boldsymbol{\delta}, \boldsymbol{\omega}) = \sum_{i=1}^{4} [0\ 1]\, \mathbf{R}(\delta_i) \mathbf{F}_i(\boldsymbol{\chi}, \delta_i, \omega_i)$, the Mean Value Theorem gives us

$$h(\boldsymbol{\chi}, \boldsymbol{\delta}, \boldsymbol{\omega}) - h(\hat{\boldsymbol{\chi}}, \boldsymbol{\delta}, \boldsymbol{\omega}) = \frac{\partial h(\boldsymbol{\chi}', \boldsymbol{\delta}, \boldsymbol{\omega})}{\partial v_y} \tilde{v}_y + \frac{\partial h(\boldsymbol{\chi}', \boldsymbol{\delta}, \boldsymbol{\omega})}{\partial r} \tilde{r} + \frac{\partial h(\boldsymbol{\chi}', \boldsymbol{\delta}, \boldsymbol{\omega})}{\partial v_x} \tilde{v}_x$$

where $\boldsymbol{\chi}'$ is some point on the line segment between $\boldsymbol{\chi}$ and $\hat{\boldsymbol{\chi}}$. Multiplying this expression with $\tilde{v}_y$, we get

$$\begin{aligned}
&\tilde{v}_y \sum_{i=1}^{4} [0\ 1]\, \mathbf{R}(\delta_i) \left(\mathbf{F}_i(\boldsymbol{\chi}, \delta_i, \omega_i) - \mathbf{F}_i(\hat{\boldsymbol{\chi}}, \delta_i, \omega_i)\right) \\
&= \sum_{i=1}^{4} \left(\cos\delta_i \frac{\partial F_{i,y}(\boldsymbol{\chi}', \delta_i, \omega_i)}{\partial v_y} + \sin\delta_i \frac{\partial F_{i,x}(\boldsymbol{\chi}', \delta_i, \omega_i)}{\partial v_y} \right) \tilde{v}_y^2 \\
&+ \sum_{i=1}^{4} \left(\cos\delta_i \frac{\partial F_{i,y}(\boldsymbol{\chi}', \delta_i, \omega_i)}{\partial r} + \sin\delta_i \frac{\partial F_{i,x}(\boldsymbol{\chi}', \delta_i, \omega_i)}{\partial r} \right) \tilde{r}\tilde{v}_y \\
&+ \sum_{i=1}^{4} \left(\cos\delta_i \frac{\partial F_{i,y}(\boldsymbol{\chi}', \delta_i, \omega_i)}{\partial v_x} + \sin\delta_i \frac{\partial F_{i,x}(\boldsymbol{\chi}', \delta_i, \omega_i)}{\partial v_x} \right) \tilde{v}_x \tilde{v}_y.
\end{aligned}$$

From Assumption 2, we arrive at (3.3a). From [11, Lemma 3.1], the Lipschitz-type condition (3.3b) holds on $X(\boldsymbol{\delta}, \boldsymbol{\omega})$ since from Assumption 2, $\mathbf{F}$ has continuous and upper bounded partial derivatives. ■

3.3 Modular observer design

3.3.1 Modular observer structure

The modular observer structure is illustrated in Figure 3.2. The first observer use information of (mainly) wheel speed in addition to yaw rate and longitudinal acceleration to estimate longitudinal velocity. Thereafter, this estimate is used together with measurements of lateral acceleration, yaw rate, wheel speeds, and wheel steering angle to estimate lateral velocity.

The measurements used are summarized below:

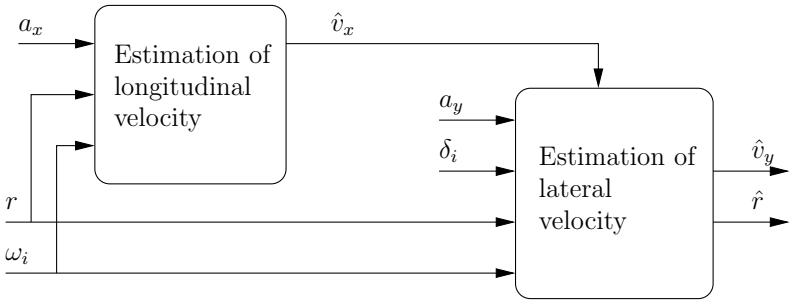

Figure 3.2: Modular observer structure

Symbol	Measurement
a_x, a_y	Longitudinal/lateral acceleration
r	yaw rate
ω_i	Rotational speed wheel i
δ_i	Steering angle wheel i

Acceleration and yaw rate sensors are assumed placed in CG. The acceleration measurements are assumed to have bias removed, and are corrected for gravity components due to vehicle roll/pitch, based on suspension stiffness and assuming a flat road.

The model described in Section 3.2 will be simplified for each of the observer modules: For estimating longitudinal velocity, we will ignore lateral (v_y and r) dynamics, and when estimating lateral dynamics, we assume that v_x is known (thus using only two dynamic states). The main motivation for structuring the observer in this way, is that it results in a modular design with few tuning knobs. Also, since we will prove stability properties independently for the modules (and thereafter overall stability), the modules can be tuned independently, and one could also imagine replacing the module for longitudinal velocity, if better estimation were available (for instance based on an observer with access to more information).

This observer structure is cascaded, since there are no feedback loops between the observers. A cascade stability result for the cascade considered herein, is given in Section 3.3.4.

3.3.2 Estimation of longitudinal velocity

In estimation of longitudinal velocity, we will use a simplified model including forward velocity only, with acceleration as input,

$$\dot{v}_x = a_x. \tag{3.4}$$

The measurements are the wheel rotational speeds ω_i, which are transformed to v_x, longitudinal velocity of CG. Assuming zero slips, we have $v_{i,x} = v_x \pm b_i r$ and $v_{i,x} = R_{dyn}\omega_i \cos\delta_i$. Denoting the transformed measurement from wheel speed i

with $v_{x,i}$, we get

$$v_{x,i} = R_{dyn}\omega_i \cos\delta_i \pm b_i r.$$

Using this, we propose the following observer:

$$\dot{\hat{v}}_x = a_x + \sum_{i=1}^{4} K_i(a_x)(v_{x,i} - \hat{v}_x). \tag{3.5}$$

The observer gains K_i depend on the longitudinal acceleration measurement, to reflect when the wheel speed measurements are good estimates of velocity, i.e., when the longitudinal tyre slips are low:

- **Large positive a_x**: Large gain on non-driven wheels, small gain on driven wheels.
- **Small positive a_x**: Very large gain on non-driven wheels, large gain on driven wheels.
- **Small negative a_x**: Large gain on non-driven wheels, large gain on driven wheels.
- **Large negative a_x**: Small gain on non-driven wheels, small gain on driven wheel.

In [13], similar rules are used to construct a Kalman filter and a fuzzy logic estimator for vehicle velocity. Other measurements (such as flags for ABS-system, brake assistant, etc.) that provide information of wheel slips can also be used. Simple outlier detection and removal is used to avoid that blocking/spinning affect the velocity estimate.

As a technical assumption for the stability results to follow, we assume that the scheduling of gains are done such that

Assumption 3 *$K_i(a_x)$ is piecewise continuous in time, and lower bounded, $K_i(a_x) > k_x > 0$.*

Assuming $v_{x,i} = v_x$ (which requires that the lateral and longitudinal slip are zero), the observer error dynamics with model (3.4) is trivially uniformly globally exponentially stable, since the gains are positive.

In general, we have slips and $v_{x,i} \neq v_x$. If the slips were known exactly, the correct equation (for each wheel) would be[1]

$$v_x = \frac{1}{1+\lambda_{i,x}} \frac{\cos(\delta_i - \alpha_i)}{\cos\alpha_i} R_{dyn}\omega_i \pm b_i r.$$

[1] One might ask if not estimates of slips can be included in the equation for $v_{x,i}$, and indeed they can, provided they are calculated from other information than the velocity estimates.

If we define $\tilde{v}_x = v_x - \hat{v}_x$, then we can write

$$\begin{aligned}\sum_{i=1}^{4} K_i(a_x)(v_{x,i} - \hat{v}_x) &= \sum_{i=1}^{4} K_i(a_x)(v_{x,i} - v_x + \tilde{v}_x) \\ &= \sum_{i=1}^{4} K_i(a_x)\tilde{v}_x + u\end{aligned}$$

where

$$u = \sum_{i=1}^{4} K_i(a_x) \left(\cos\delta_i - \frac{1}{1+\lambda_{i,x}} \frac{\cos(\delta_i - \alpha_i)}{\cos\alpha_i} \right) R_{dyn}\omega_i$$

is an error-term due to non-zero slip. When the slips are zero, then $u(t) = 0$. Consequently, the error dynamics are

$$\dot{\tilde{v}}_x = -\sum_{i=1}^{4} K_i(a_x)\tilde{v}_x + u. \tag{3.6}$$

We already know that with $u = 0$, we have global exponential stability. But during accelerations (including turning and braking), $u \neq 0$, and will influence the observer error. Natural properties to aim for, are that the influence u on $\tilde{v}_x$ should not lead to divergence of the estimate, when u is small the influence on the estimate should be small, and that when u vanishes, $\tilde{v}_x$ should go to zero. These properties correspond to input-to-state stability (ISS) [21, 11], characterized by convergence of zero-input response, and that the zero state response is bounded for bounded input.

Theorem 1 *If the wheel speeds, steering angles and vehicle velocity are bounded, the observer error dynamics (3.6) are globally ISS with respect to $u(t)$, and*

$$|\tilde{v}_x(t)| \leq |\tilde{v}_x(t_0)| e^{-\frac{k_x}{2}(t-t_0)} + \frac{2}{k_x} \left(\sup_{t_o \leq \tau \leq t} |u(\tau)| \right). \tag{3.7}$$

PROOF Boundedness of wheel speeds, steering angle and vehicle velocity implies that $\sup_{t_o \leq \tau \leq t} |u(\tau)|$ exists. Then (3.7) follows from (3.6), which again implies global ISS [11, Definition 4.7]. ■

Note that we have disregarded the Coriolis term in the observer model (3.4) and analysis. However, the effect of the Coriolis term could be included in $u(t)$, also giving ISS.

3.3.3 Estimation of lateral velocity

In estimating the lateral velocity, we will first consider the estimate of longitudinal velocity $\hat{v}_x$ as the true longitudinal velocity v_x, a time-varying parameter. In Section 3.3.4, this assumption is removed, by analyzing both observers together.

Thus, in this section we let $\mathbf{x} = (v_y, r)^\mathsf{T}$ and lump the parameters in $\theta = (v_x, \delta^\mathsf{T}, \omega^\mathsf{T})^\mathsf{T}$. We assume further that the road is flat (no road bank and inclination angle), and that the friction model is time-invariant and known. The model we use here is then[2]

$$\dot{v}_y = -v_x r + a_y \tag{3.8a}$$

$$\dot{r} = \frac{1}{J_z} \sum_{i=1}^{4} \mathbf{g}_i^\mathsf{T} \mathbf{R}(\delta_i) \mathbf{F}_i \tag{3.8b}$$

Based on this model, we propose the following observer:

$$\dot{\hat{v}}_y = -v_x r + a_y - K_{v_y} \left(m a_y - \sum_{i=1}^{4} [0\ 1]\, \mathbf{R}(\delta_i) \hat{\mathbf{F}}_i \right) \tag{3.9a}$$

$$\dot{\hat{r}} = \frac{1}{J_z} \sum_{i=1}^{4} \mathbf{g}_i^\mathsf{T} \mathbf{R}(\delta_i) \hat{\mathbf{F}}_i + K_r \left(r - \hat{r} \right). \tag{3.9b}$$

Define the error variables $\tilde{v}_y = v_y - \hat{v}_y$ and $\tilde{r} = r - \hat{r}$, and $\tilde{\mathbf{x}} = (\tilde{v}_y, \tilde{r})^\mathsf{T}$. We will make use of the following fact:

Fact 1 *By completing the squares,*

$$-a\xi_1^2 + b|\xi_1||\xi_2| = \frac{b^2}{4a}\xi_2^2 - \left(\sqrt{a}|\xi_1| - \frac{b}{2\sqrt{a}}|\xi_2| \right)^2$$

Define (with some abuse of notation) the sets $X(\boldsymbol{\theta}) := \{\mathbf{x} : (v_x, \mathbf{x}) \in X(\boldsymbol{\delta}, \boldsymbol{\omega})\}$ and[3] $X_s(\rho; \boldsymbol{\theta}) = \{\mathbf{x} : B(\mathbf{x}, \rho) \subset X(\boldsymbol{\theta})\} \subset X(\boldsymbol{\theta})$.

Theorem 2 *Assume that ρ and Θ are such that $\mathbf{x}(t) \in X_s(\rho; \boldsymbol{\theta})$, $\forall \boldsymbol{\theta} \in \Theta$, $\forall t > 0$. For some $k_r > 0$, let the observer gains be chosen such that*

$$K_{v_y} > 0 \tag{3.10}$$

$$K_r > k_r + c_5 + \frac{(K_{v_y} c_2 + c_4)^2}{2 K_{v_y} c_1}. \tag{3.11}$$

Then, if $||\tilde{\mathbf{x}}(0)|| \leq \rho$, the state $\hat{\mathbf{x}}(t)$ of the observer (3.9) converges to the state $\mathbf{x}(t)$ of the system (3.8), and the origin of the observer error dynamics is uniformly exponentially stable. □

Proof The observer error dynamics are

$$\dot{\tilde{v}}_y = K_{v_y} \sum_{i=1}^{4} [0\ 1]\, \mathbf{R}(\delta_i)(\mathbf{F}_i - \hat{\mathbf{F}}_i) \tag{3.12a}$$

$$\dot{\tilde{r}} = \frac{1}{J_z} \sum_{i=1}^{4} \mathbf{g}_i^\mathsf{T} \mathbf{R}(\delta_i)(\mathbf{F}_i - \hat{\mathbf{F}}_i) - K_r \tilde{r}. \tag{3.12b}$$

[2] For brevity, we use $\mathbf{F}_i$ for $\mathbf{F}_i(v_x, v_y, r, \delta_i, \omega_i)$ and $\hat{\mathbf{F}}_i$ for $\mathbf{F}_i(v_x, \hat{v}_y, \hat{r}, \delta_i, \omega_i)$ in this section.

[3] $B(\mathbf{x}, \rho) := \{\mathbf{z} : \|\mathbf{z} - \mathbf{x}\| \leq \rho\}$ is the ball of radius ρ around $\mathbf{x}$.

Define the Lyapunov function candidate $V(\tilde{\mathbf{x}}) = \frac{1}{2}(\tilde{v}_y^2 + \tilde{r}^2)$. The time derivative along the trajectories of (3.12) is

$$\dot{V} = \tilde{v}_y \left(K_{v_y} \sum_{i=1}^{4} [0\ 1]\, \mathbf{R}(\delta_i)(\mathbf{F}_i - \hat{\mathbf{F}}_i) \right) + \tilde{r} \left(\frac{1}{J_z} \sum_{i=1}^{4} \mathbf{g}_i^{\mathsf{T}} \mathbf{R}(\delta_i)(\mathbf{F}_i - \hat{\mathbf{F}}_i) - K_r \tilde{r} \right).$$

Letting $\hat{v}_x = v_x$ in Lemma 1, the following holds on $X(\boldsymbol{\delta}, \boldsymbol{\omega})$:

$$\begin{aligned} \tilde{v}_y \sum_{i=1}^{4} [0\ 1]\, \mathbf{R}(\delta_i) \left(\mathbf{F}_i - \hat{\mathbf{F}}_i \right) &\leq -c_1 \tilde{v}_y^2 + c_2 |\tilde{r}||\tilde{v}_y| \frac{1}{J_z} \sum_{i=1}^{4} \mathbf{g}_i^{\mathsf{T}} \mathbf{R}(\delta_i) \left(\mathbf{F}_i - \hat{\mathbf{F}}_i \right) \\ &\leq c_4 |\tilde{v}_y| + c_5 |\tilde{r}| \end{aligned}$$

Using this, $\dot{V}$ can be upper bounded:

$$\begin{aligned} \dot{V} &\leq -K_{v_y} c_1 \tilde{v}_y^2 + K_{v_y} c_2 |\tilde{r}||\tilde{v}_y| + c_4 \tilde{r}|\tilde{v}_y| + c_5 \tilde{r}|\tilde{r}| - K_r \tilde{r}^2. \\ &\leq (K_{v_y} c_2 + c_4)|\tilde{r}||\tilde{v}_y| - K_{v_y} c_1 \tilde{v}_y^2 + c_5 \tilde{r}|\tilde{r}| - K_r \tilde{r}^2. \end{aligned}$$

By Fact 1 and (3.10),

$$\dot{V} \leq \frac{(K_{v_y} c_2 + c_4)^2}{2 K_{v_y} c_1} \tilde{r}^2 - \frac{K_{v_y} c_1}{2} \tilde{v}_y^2 + c_5 \tilde{r}|\tilde{r}| - K_r \tilde{r}^2 - \left(\sqrt{\frac{K_{v_y} c_1}{2}} |\tilde{v}_y| - \frac{(K_{v_y} c_2 + c_4)}{\sqrt{2 K_{v_y} c_1}} |\tilde{r}| \right)^2$$

We see that due to (3.11),

$$\dot{V} \leq -\frac{K_{v_y} c_1}{2} \tilde{v}_y^2 - k_r \tilde{r}^2 \tag{3.13}$$

is uniformly negative definite for $\mathbf{x}, \hat{\mathbf{x}} \in X(\boldsymbol{\theta})$. By assumption, $\mathbf{x}(t) \in X_s(\rho, \boldsymbol{\theta}(t)) \subset X(\boldsymbol{\theta}(t))\ \forall t > 0$, and we must show that $\hat{\mathbf{x}}(t) \in X(\boldsymbol{\theta}(t))\ \forall t > 0$. Since $\mathbf{x}(t) \in X_s(\rho; \boldsymbol{\theta})$ and $||\tilde{\mathbf{x}}(0)|| \leq \rho$, $\hat{\mathbf{x}}(0) \in X(\boldsymbol{\theta}(0))$. From the above, $\frac{d}{dt}||\tilde{\mathbf{x}}|| = \frac{\dot{V}}{||\tilde{\mathbf{x}}||} < 0$, which means that $\|\tilde{\mathbf{x}}(t)\| \leq \rho\ \forall t > 0$, and thus $\hat{\mathbf{x}}(t)$ will remain in $X(\boldsymbol{\theta}(t))$. Thus, from (3.13) and standard Lyapunov theory [11], we conclude that $\tilde{\mathbf{x}}(t) \to 0$ with exponential convergence rate. ■

Remark 2 Note that the observer for $\hat{v}_y$ could use the estimate $\hat{r}$ instead of the measured r in the Coriolis term, that is, $\dot{\hat{v}}_y = -v_x \hat{r} + a_y - K_{v_y} \left(m a_y - \sum_{i=1}^{4} [0\ 1]\, \mathbf{R}(\delta_i) \hat{\mathbf{F}}_i \right)$, with only slight changes to the proof above (the main difference being that the upper bound (3.11) will depend on an upper bound on v_x. See [8]). □

3.3.4 Cascaded stability

In the previous section, we assumed we knew the real velocity v_x. In this section, we analyze the stability properties since we have to use the estimate, $\hat{v}_x$, instead of v_x.

Since $\hat{v}_x = v_x - \tilde{v}_x$, the lateral velocity observer error dynamics can be written[4]

$$\dot{\tilde{v}}_y = K_{v_y} \sum_{i=1}^{4} [0\ 1]\, \mathbf{R}(\delta_i)(\mathbf{F}_i - \hat{\mathbf{F}}_i) - \tilde{v}_x r$$
$$\dot{\tilde{r}} = \frac{1}{J_z} \sum_{i=1}^{4} \mathbf{g}_i^{\mathsf{T}} \mathbf{R}(\delta_i)(\mathbf{F}_i - \hat{\mathbf{F}}_i) - K_r \tilde{r}.$$

Using the Lyapunov function from the proof of Theorem 2, letting $k_y = \min\left(K_{v_y} c_1/2, k_r\right)$, we have

$$\begin{aligned}\dot{V} &\leq -\frac{K_{v_y} c_1}{2} \tilde{v}_y^2 - k_r \tilde{r}^2 + |\tilde{v}_y||r||\tilde{v}_x| + c_3 |\tilde{v}_y||\tilde{v}_x| + c_6 |\tilde{r}||\tilde{v}_x| \\ &\leq -k_y \|\tilde{\mathbf{x}}\|^2 + \kappa \|\tilde{\mathbf{x}}\||\tilde{v}_x|\end{aligned}$$

where $\kappa = \sqrt{2} \max\left(\bar{r} + c_3, c_6\right)$, and $\bar{r}$ is an upper bound on $r(t)$. By this, it follows that

$$\dot{V} \leq -\frac{k_y}{2} \|\tilde{\mathbf{x}}\|^2, \quad \forall\ \|\tilde{\mathbf{x}}\| \geq \frac{2\kappa}{k_y} |\tilde{v}_x|$$

implying ISS by [11, Theorem 4.19], namely, that

$$\|\tilde{\mathbf{x}}(t)\| \leq \|\tilde{\mathbf{x}}(t_0)\| e^{-\frac{k_y}{2}(t - t_0)} + \frac{2\kappa}{k_y} \left(\sup_{t_o \leq \tau \leq t} |\tilde{v}_x(\tau)| \right) \tag{3.14}$$

assuming the supremum exists, and that $\tilde{\mathbf{x}}(t) \to 0$ if $\tilde{v}_x(t) \to 0$ as $t \to \infty$. However, since the conditions of Theorem 2 do not hold globally, we use a local variant of ISS:

Corollary 1 *Assume that the conditions of Theorem 2 holds for all* $(\boldsymbol{\delta}, \boldsymbol{\omega}) \in \Delta \times \Omega$ *on* $\|\tilde{\mathbf{x}}\| \leq r$ *and* $|u| \leq r_u$. *Then there exists positive constants* k_1 *and* k_2 *such that (3.14) holds for* $\|\tilde{\mathbf{x}}(t_0)\| < k_1$ *and* $\sup_{t > t_0} |u(t)| < k_2$. □

PROOF Follows from local ISS [11, p. 192] and the above. ■

The cascaded stability is illustrated in Figure 3.3.

3.4 Combined observer design

In this section, we combine longitudinal and lateral velocity estimation in the same observer, and thus let $\mathbf{x} = (v_x, v_y, r)^{\mathsf{T}}$. The major advantage is that the Coriolis

[4] Where $\hat{\mathbf{F}}_i$ now is used for $\mathbf{F}_i(\hat{v}_x, \hat{v}_y, \hat{r}, \delta_i, \omega_i)$.

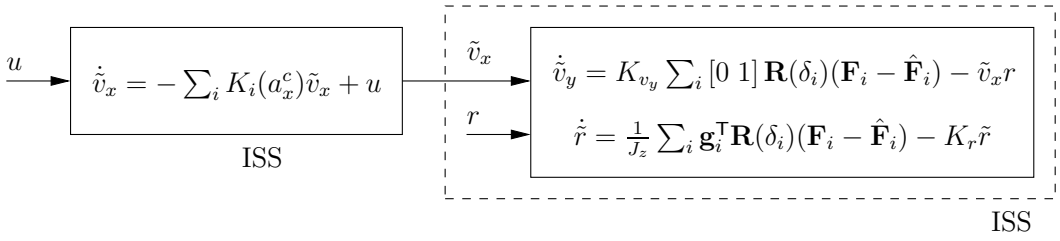

Figure 3.3: Stability properties of observer error dynamics

term can be included in the equation for longitudinal velocity. The system equations in this case, are then[5]

$$\begin{aligned}\dot{v}_x &= v_y r + a_x\\ \dot{v}_y &= -v_x r + a_y\\ \dot{r} &= \frac{1}{J_z}\sum_{i=1}^{4}\mathbf{g}_i^\mathsf{T}\mathbf{R}(\delta_i)\mathbf{F}_i,\end{aligned}$$

for which we propose the following observer:

$$\dot{\hat{v}}_x = \hat{v}_y r + a_x + \sum_{i=1}^{4} K_i(a_x)(v_{x,i} - \hat{v}_x) \tag{3.15a}$$

$$\dot{\hat{v}}_y = -\hat{v}_x r + a_y - K_{v_y}\left(ma_y - \sum_{i=1}^{4}[0\ 1]\,\mathbf{R}(\delta_i)\hat{\mathbf{F}}_i\right) \tag{3.15b}$$

$$\dot{\hat{r}} = \frac{1}{J_z}\sum_{i=1}^{4}\mathbf{g}_i^\mathsf{T}\mathbf{R}(\delta_i)\hat{\mathbf{F}}_i + K_r\,(r - \hat{r})\,. \tag{3.15c}$$

As in Section 3.3.2, we write

$$\sum_{i=1}^{4} K_i(a_x)(v_{x,i} - \hat{v}_x) = \sum_{i=1}^{4} K_i(a_x)\tilde{v}_x + u.$$

and thus the goal of this section is to show that the observer error dynamics,

$$\dot{\tilde{v}}_x = \tilde{v}_y r - \sum_{i=1}^{4} K_i(a_x)\tilde{v}_x + u \tag{3.16a}$$

$$\dot{\tilde{v}}_y = -\tilde{v}_x r + K_{v_y}\sum_{i=1}^{4}[0\ 1]\,\mathbf{R}(\delta_i)(\mathbf{F}_i - \hat{\mathbf{F}}_i) \tag{3.16b}$$

$$\dot{\tilde{r}} = \frac{1}{J_z}\sum_{i=1}^{4}\mathbf{g}_i^\mathsf{T}\mathbf{R}(\delta_i)(\mathbf{F}_i - \hat{\mathbf{F}}_i) - K_r\tilde{r} \tag{3.16c}$$

are ISS with $u(t)$ as input.

[5] In this section we use $\mathbf{F}_i$ for $\mathbf{F}_i(v_x, v_y, r, \delta_i, \omega_i)$ and $\hat{\mathbf{F}}_i$ for $\mathbf{F}_i(\hat{v}_x, \hat{v}_y, \hat{r}, \delta_i, \omega_i)$.

For the purposes of this section, we redefine $X_s(\rho;\boldsymbol{\delta},\boldsymbol{\omega}) = \{\mathbf{x} : B(\mathbf{x},\rho) \subset X(\boldsymbol{\delta},\boldsymbol{\omega})\} \subset X(\boldsymbol{\delta},\boldsymbol{\omega})$. We first show that with $u(t) = 0$, the observer is exponentially stable:

Theorem 3 *Assume that ρ and Δ, Ω are such that $\mathbf{x}(t) \in X_s(\rho;\boldsymbol{\delta},\boldsymbol{\omega})$, $\forall(\boldsymbol{\delta},\boldsymbol{\omega}) \in \Delta\times\Omega$, $\forall t > 0$, and that $u(t) = 0$, $\forall t > 0$. Let the observer gains be chosen such that*

$$K_{v_y} > 0 \tag{3.16d}$$

$$k_x > \frac{1}{4}\frac{K_{v_y}c_3^2}{c_1} \tag{3.16e}$$

$$K_r > c_5 + \frac{c_7}{4k_xK_{v_y}c_1 - (K_{v_y}c_3)^2} \tag{3.16f}$$

where

$$c_7 = (K_{v_y}c_2 + c_4)(k_x(K_{v_y}c_2 + c_4) - \frac{1}{2}K_{v_y}c_3c_6) + c_6(\frac{1}{2}K_{v_y}c_3(K_{v_y}c_2 + c_4) + K_{v_y}c_1c_6).$$

Then, if $||\tilde{\mathbf{x}}(0)|| \le \rho$, the state $\hat{\mathbf{x}}(t)$ of the observer (3.9) converges to the state $\mathbf{x}(t)$ of the system (3.8), and the origin of the observer error dynamics (3.16) is uniformly exponentially stable. □

PROOF Define the Lyapunov function candidate $V(\tilde{\mathbf{x}}) = \frac{1}{2}(\tilde{v}_x^2 + \tilde{v}_y^2 + \tilde{r}^2)$. The time derivative along the trajectories of the error dynamics (3.16) is

$$\begin{aligned}\dot{V} = {} & \tilde{v}_x\left(\tilde{v}_y r - \sum_{i=1}^{4} K_i(a_x)\tilde{v}_x\right) \\ & + \tilde{v}_y\left(-\tilde{v}_x r + K_{v_y}\sum_{i=1}^{4}[0\ 1]\,\mathbf{R}(\delta_i)(\mathbf{F}_i - \hat{\mathbf{F}}_i)\right) \\ & + \tilde{r}\left(\frac{1}{J_z}\sum_{i=1}^{4}\mathbf{g}_i^{\mathsf{T}}\mathbf{R}(\delta_i)(\mathbf{F}_i - \hat{\mathbf{F}}_i) - K_r\tilde{r}\right).\end{aligned}$$

Using Lemma 1, this can be upper bounded:

$$\begin{aligned}\dot{V} &\le -k_x\tilde{v}_x^2 - K_{v_y}c_1\tilde{v}_y^2 + K_{v_y}c_2|\tilde{r}||\tilde{v}_y| + K_{v_y}c_3|\tilde{v}_x||\tilde{v}_y| \\ &\quad + c_4\tilde{r}|\tilde{v}_y| + c_5\tilde{r}|\tilde{r}| + c_6\tilde{r}|\tilde{v}_x| - K_r\tilde{r}^2 \\ &= -|\tilde{\mathbf{x}}|^{\mathsf{T}}A|\tilde{\mathbf{x}}|,\end{aligned}$$

where $|\tilde{\mathbf{x}}|$ and the matrix A are defined as

$$|\tilde{\mathbf{x}}| := \begin{pmatrix}|\tilde{v}_x| \\ |\tilde{v}_y| \\ |\tilde{r}|\end{pmatrix},\ A := \begin{pmatrix}k_x & -\frac{1}{2}K_{v_y}c_3 & -\frac{1}{2}c_6 \\ -\frac{1}{2}K_{v_y}c_3 & K_{v_y}c_1 & -\frac{1}{2}K_{v_y}c_2 - \frac{1}{2}c_4 \\ -\frac{1}{2}c_6 & -\frac{1}{2}K_{v_y}c_2 - \frac{1}{2}c_4 & K_r - c_5\end{pmatrix}.$$

To show that $\dot{V} < 0$, we show how the conditions (3.16d)-(3.16f) imply that all principal minors of A are positive, and thus that A is positive definite. The second

principal minor is $k_x K_{v_y} c_1 - \frac{1}{4}(K_{v_y} c_3)^2$. We see that due to (3.16d), this is positive due to (3.16e), which also ensures the positivity of the first principal minor (k_x). The third principal minor (the determinant of A) is (developed after the third column)

$$(K_r - c_5)\left(k_x K_{v_y} c_1 - \frac{1}{4}(K_{v_y} c_3)^2\right) + \frac{1}{2}(K_{v_y} c_2 + c_4)\det A_{2,3} - \frac{1}{2} c_6 \det A_{1,3}$$

where $A_{i,j}$ is the 2×2 matrix produced by removing row i and column j from A. Noting that $\det A_{2,3}$ and $\det A_{1,3}$ do not depend on K_r, we see that this determinant can be made positive by choosing K_r large enough. Doing the tedious calculations, we end up with the bound (3.16f). The rest follows as in Theorem 2. ■

Using the Lyapunov function in the above proof, a non-zero $u(t)$ gives (for small $\tilde{\mathbf{x}}$)

$$\dot{V} \leq -\lambda_{\min}(A)\|\tilde{\mathbf{x}}\|^2 + \|\tilde{\mathbf{x}}\||u|$$

which shows that

$$\dot{V} \leq -\frac{\lambda_{\min}(A)}{2}\|\tilde{\mathbf{x}}\|^2, \quad \forall\, \|\tilde{\mathbf{x}}\| \geq \frac{2}{\lambda_{\min}(A)}|u|$$

implying

$$\|\tilde{\mathbf{x}}(t)\| \leq \|\tilde{\mathbf{x}}(t_0)\| e^{-\frac{\lambda_{\min}(A)}{2}(t-t_0)} + \frac{2}{\lambda_{\min}(A)}\left(\sup_{t_o \leq \tau \leq t} |u(\tau)|\right) \tag{3.17}$$

assuming the supremum exists. Since the conditions in Theorem 3 do not hold globally, we conclude as in Section 3.3.4 a local variant of ISS:

Corollary 2 *Assume that the conditions of Theorem 3 holds for all* $(\boldsymbol{\delta}, \boldsymbol{\omega}) \in \Delta \times \Omega$ *on* $\|\tilde{\mathbf{x}}\| \leq r$ *and* $|u| \leq r_u$. *Then there exists positive constants* k_1 *and* k_2 *such that (3.17) holds for* $\|\tilde{\mathbf{x}}(t_0)\| < k_1$ *and* $\sup_{t>t_0} |u(t)| < k_2$. □

3.5 Discussion of Assumption 2

This section discusses Assumption 2 for two friction models. Most friction models can be written as a function of (lateral and longitudinal) tyre slips $\mathbf{F}_i = \mathbf{F}_i(\lambda_{i,x}, \lambda_{i,y})$ only[6], and depend thus on vehicle velocity only indirectly. Therefore, we can write the partial derivatives

$$\frac{\partial F_{i,x}}{\partial v_y} = \frac{\partial F_{i,x}}{\partial \lambda_{i,x}}\frac{\partial \lambda_{i,x}}{\partial v_y} + \frac{\partial F_{i,x}}{\partial \lambda_{i,y}}\frac{\partial \lambda_{i,y}}{\partial v_y} = \frac{\partial F_{i,x}}{\partial \lambda_{i,y}}\cos\alpha_i \frac{\partial \alpha_i}{\partial v_y}$$
$$\frac{\partial F_{i,y}}{\partial v_y} = \frac{\partial F_{i,y}}{\partial \lambda_{i,x}}\frac{\partial \lambda_{i,x}}{\partial v_y} + \frac{\partial F_{i,y}}{\partial \lambda_{i,y}}\frac{\partial \lambda_{i,y}}{\partial v_y} = \frac{\partial F_{i,y}}{\partial \lambda_{i,y}}\cos\alpha_i \frac{\partial \alpha_i}{\partial v_y}$$

where we have assumed $\frac{\partial \lambda_{i,x}}{\partial v_y} = 0$. Since

$$\frac{\partial \alpha_i}{\partial v_y} = \frac{-1}{1 + \tan^2(\delta_i - \alpha_i)} < 0,$$

we see that it is the lateral slip partial derivatives that are significant (assuming $\alpha_i < \pi/2$).

[6]Some may depend on tyre slip angle α_i or $\tan\alpha_i$ instead of $\lambda_{i,y} = \sin\alpha_i$, but this does not change the analysis.

3.5.1 Linear friction models

Linear friction models says that the friction forces are proportional to the slips,

$$\begin{pmatrix} F_{i,x}(\lambda_{x,i}, \lambda_{y,i}) \\ F_{i,y}(\lambda_{x,i}, \lambda_{y,i}) \end{pmatrix} = \begin{pmatrix} C_x \lambda_{i,x} \\ C_y \lambda_{i,y} \end{pmatrix}$$

where C_x and C_y are tyre (slip and cornering) stiffness coefficients. We conclude that Assumption 2 holds as discussed in Remark 1, for some $\bar{\alpha} < \pi/2$.

3.5.2 The magic formula tyre model

The "magic formula tyre model" [17] is a widely used semi-empirical model for calculating steady-state tyre forces. The "combined slip" magic formula provides similar formulas for lateral and longitudinal tyre forces,

$$\begin{aligned} F_x(\lambda_x, \lambda_y) &= G_x(\lambda_y) F_{x0}(\lambda_x), \\ F_y(\lambda_x, \lambda_y) &= G_y(\lambda_x) F_{y0}(\lambda_y) \end{aligned}$$

where we have simplified somewhat since one of the parameters in G_x (G_y) that according to [17] depends on λ_x (λ_y) is assumed constant. Furthermore, we use $\lambda_y = \sin\alpha$ instead of $\tan\alpha$, but this is not significant for the conclusions drawn here. For notational convenience we drop the dependence on wheel index i in this section.

The functions F_{x0} and F_{y0} are the "pure slip" formulas,

$$F_{x0}(\lambda_x) = D_x \sin\zeta_x, \quad F_{y0}(\lambda_y) = D_y \sin\zeta_y$$

where

$$\begin{aligned} \zeta_x &= C_x \arctan\{B_x\lambda_x - E_x(B_x\lambda_x - \arctan B_x\lambda_x)\} \\ \zeta_y &= C_y \arctan\{B_y\lambda_y - E_y(B_y\lambda_y - \arctan B_y\lambda_y)\}. \end{aligned}$$

The functions G_x and G_y are defined as $G_x(\lambda_y) = \cos\eta_x$ and $G_y(\lambda_x) = \cos\eta_y$ where

$$\begin{aligned} \eta_x &= C_{Gx} \arctan\{B_{Gx}\lambda_y - E_{Gx}(B_{Gx}\lambda_y - \arctan B_{Gx}\lambda_y)\} \\ \eta_y &= C_{Gy} \arctan\{B_{Gy}\lambda_x - E_{Gy}(B_{Gy}\lambda_x - \arctan B_{Gy}\lambda_x)\}. \end{aligned}$$

We then have that

$$\frac{\partial F_y}{\partial \lambda_y} = G_y(\lambda_x) \frac{B_y C_y D_y \left(1 - E_y\left(1 - \frac{1}{1+B_y^2\lambda_y^2}\right)\right)\cos\zeta_y}{1+\zeta_y^2}.$$

Since $G(\lambda_x) > 0$ and $E_y \leq 1$ [17, p. 189], $\frac{\partial F_y}{\partial \lambda_y} > 0$ for $\zeta_y < \pi/2$. For "shape factor" $C_y < 1$, this holds for all λ_y. For $C_y > 1$, the friction force declines for large λ_ys, and $\frac{\partial F_y}{\partial \lambda_y} > 0$ only to the left of the peak of the friction curve, that is, for $|\lambda_y| \leq \bar{\lambda}$ where $\bar{\lambda}$ is defined by

$$E_y = \frac{B_y\bar{\lambda} - \tan\frac{\pi}{2C_y}}{B_y\bar{\lambda} - \arctan(B_y\bar{\lambda})}.$$

Furthermore,

$$\frac{\partial F_x}{\partial \lambda_y} = -F_{x0}(\lambda_x)\frac{B_{Gx}C_{Gx}\left(1-E_{Gx}\left(1-\frac{1}{1+B_{Gx}^2\lambda_y^2}\right)\right)\sin\eta_x}{1+\eta_x^2}$$

We see that $\operatorname{sign}\frac{\partial F_x}{\partial \lambda_y} = -\operatorname{sign}(\lambda_x\lambda_y)$ (since $\operatorname{sign} F_{x0}(\lambda_x) = \operatorname{sign}\zeta_x = \operatorname{sign}\lambda_x$ and $\operatorname{sign}\eta_x = \operatorname{sign}\lambda_y$).

From the above, we make the following observations:

- For sufficiently small side-slip angles (that is, $|\lambda_y| < \bar{\lambda}$) and small δ, the first part of (3.2) is negative and dominates the second part.
- For $\lambda_x \approx 0$ the second part of (3.2) is approximately zero, and hence dominated by the first part.
- For large side-slip angles, the first part of (3.2) will get less negative, and even positive if $C_y > 1$. However, in the case of braking ($\lambda_x < 0$), then the second part of (3.2) will often contribute in fulfilling the assumption: Since $\operatorname{sign}\frac{\partial F_x}{\partial v_y} = \operatorname{sign}\lambda_x \operatorname{sign}\alpha$, assuming that $\operatorname{sign}\alpha = \operatorname{sign}\delta$, gives $\frac{\partial F_x}{\partial v_y}\sin\delta < 0$.

In conclusion, (3.2) is negative for realistic slip values and sufficiently small steering angles for tyres with $C_y < 1$. For tyres with $C_y > 1$, then for some combinations of λ_x and (large) λ_y, it might be positive. Since it is the sum for all tyres that should be negative, a positive summand for one (or two) wheel(s) might be weighed against negative summands for the other wheels (for instance, rear wheels will often have lower side-slip angles due to small steering angle values). Finally, we remark that Assumption 2 is merely a (conservative) *sufficient* condition for stability.

3.5.3 Convergence monitoring

When a friction model is available, then (3.2) can be evaluated based on the estimates, either online or offline. Since (3.2) essentially is the only assumption that is required for the analysis herein, the value can be used for convergence monitoring, somewhat akin to monitoring covariances in an EKF, and corrective steps can be taken when the value becomes positive.

3.6 Experimental results

In this section, the observers are applied to experimental data from a car. The velocity estimates ($\hat{v}_x$, $\hat{v}_y$, and side slip angle $\hat{\beta} = \arctan(-\hat{v}_y/\hat{v}_x)$) are compared to velocity measurements obtained using an optical sensor placed in front of the vehicle.

The gains of the observers are the same in all experiments. The gains in the longitudinal velocity observer vary between 0 and 200 (but such that $\sum_{i=0}^{4} K_i(a_x) > 0$ always), and $K_{v_y} = 1/m$ and $K_r = 20$.

Initial conditions for the observers are one of the wheel speeds (transformed to CG) for $\hat{v}_x$, and 0 for $\hat{v}_y$ and $\hat{r}$. Experimenting with the initial conditions indicate

a large region of attraction (divergence was not observed as long as the choice of maximum friction coefficient μ_H in the friction model is reasonable).

3.6.1 Modular observer

Flat dry road, slalom maneuver

The maximum friction coefficient used in the observer is set to $\mu_H = 1$. The longitudinal velocity is shown in Fig. 3.4, while lateral velocity is shown in Fig. 3.5. The quality of both estimates are fine, so the vehicle side slip estimate, shown in Fig. 3.6, is also good.

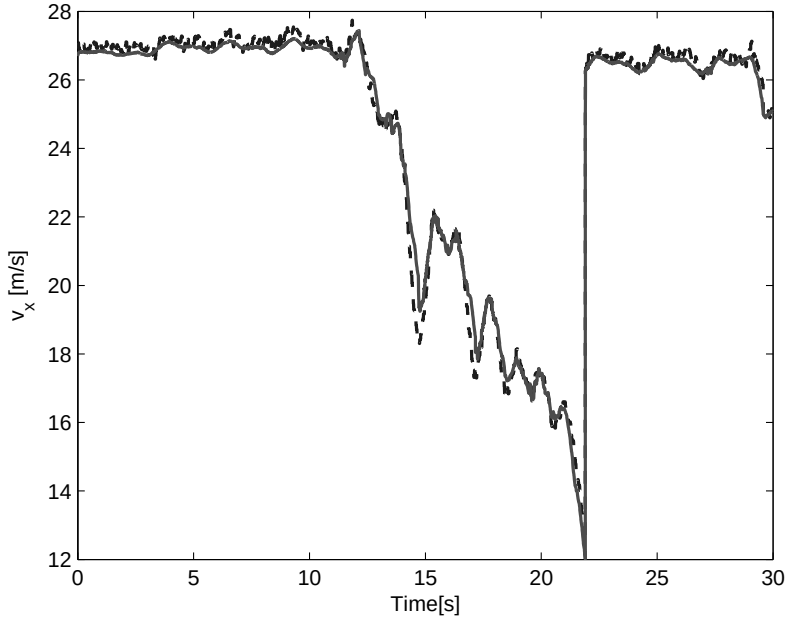

Figure 3.4: Estimate (solid) and measurement (dashed) of longitudinal velocity, slalom maneuver.

Ice, driving in circle

The maximum friction coefficient used in the observer is set to $\mu_H = 0.3$. The longitudinal velocity is shown in Fig. 3.7. The estimate is noisy, mainly due to large variations in the wheel speed measurements (caused by varying longitudinal slips). The estimate is rather inaccurate between 16.5-17.5s. This is when the lateral velocity is at its highest, and inspection of the wheel speed measurements reveals that three of four wheels give a bad indication of vehicle velocity. In this situation the "open loop" strategy of integrating longitudinal acceleration (induced by low gains in wheel velocity injection terms) is not improving the estimate, since the Coriolis term (not taken into account in the modular approach) dominates the longitudinal acceleration.

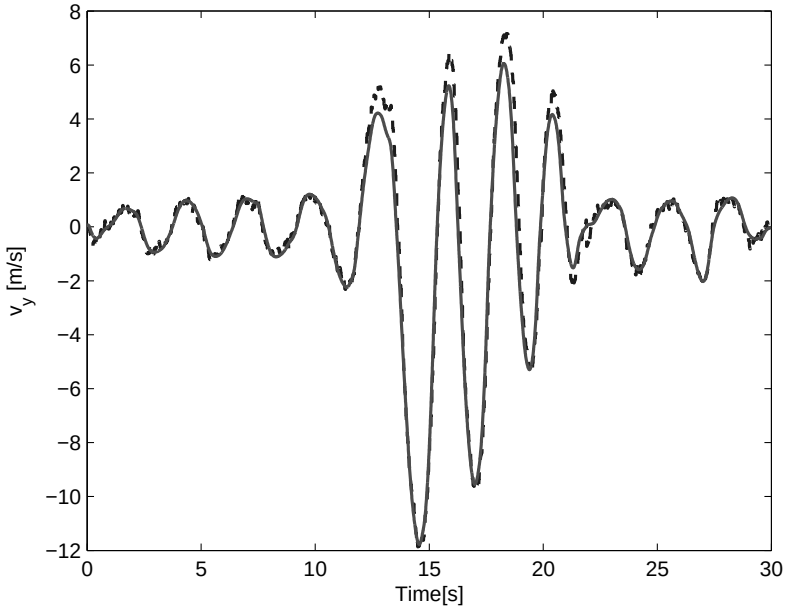

Figure 3.5: Estimate (solid) and measurement (dashed) of lateral velocity, slalom maneuver.

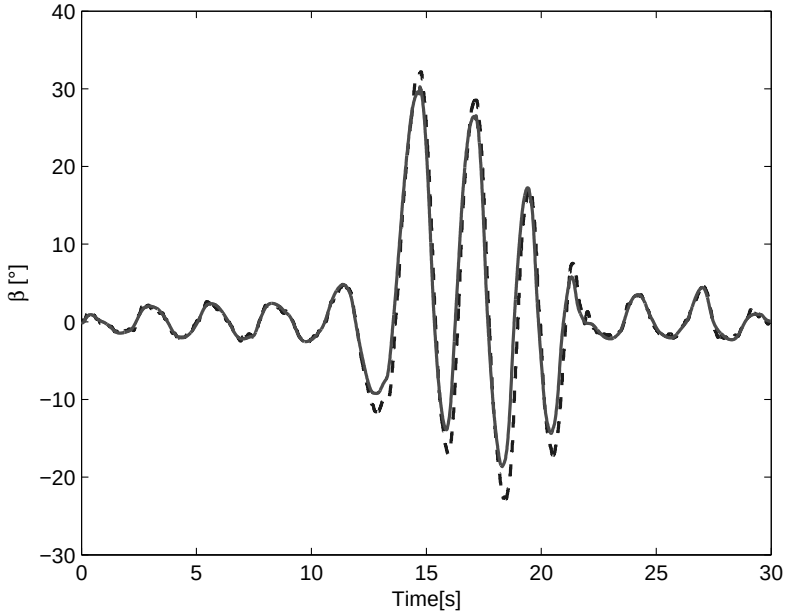

Figure 3.6: Estimate (solid) and measurement (dashed) of side slip, slalom maneuver.

The lateral velocity is shown in Fig. 3.8. The quality of this estimate is acceptable, as is the vehicle side slip angle estimate, Fig. 3.9. The reason for lower quality estimates in this experiment is mainly due to that the friction model may be less accurate on ice, combined with larger slip values. Another reason is that driving in circle may be a more difficult maneuver to estimate.

It should also be mentioned that the optical measurements of velocity might exhibit larger errors in this experiment, compared with the first experiment.

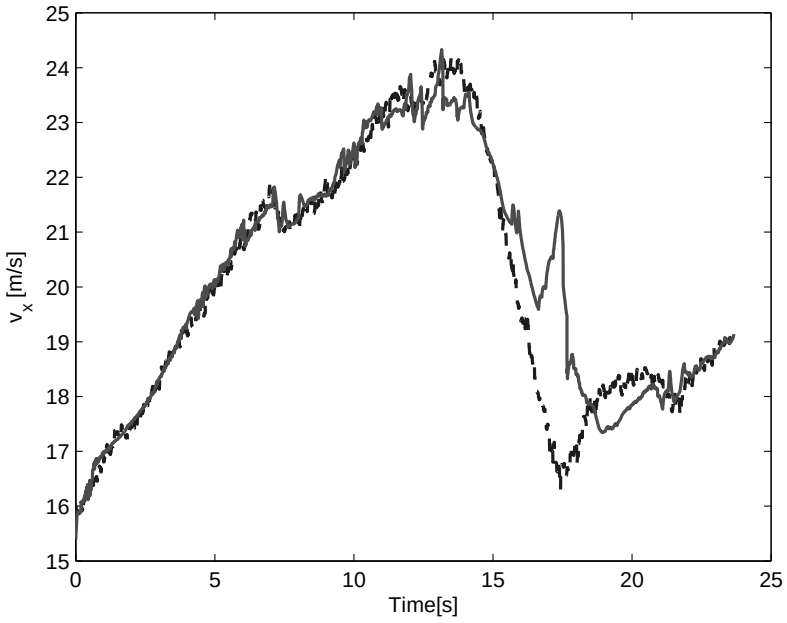

Figure 3.7: Estimate (solid) and measurement (dashed) of longitudinal velocity, circle on ice, modular observer.

3.6.2 Combined observer

The data from the ice maneuver is also run through the full observer design (Section 3.4), see figures 3.10-3.12. The slalom on dry road-data are omitted, since the results are essentially indistinguishable from the modular observer in Section 3.6.1.

We can see that in the period around 16 seconds, the longitudinal velocity estimate is considerably improved. In this period, there is a large negative longitudinal acceleration, which means the observer puts little weight on wheel speed measurement and instead integrates the lateral acceleration and the Coriolis term. It is the inclusion of the Coriolis term that has improved the estimate compared with the modular approach.

In the same period, the lateral velocity estimate has apparently become worse than in the cascaded approach. However, the better estimate in the cascaded observer is probably due to "luck", the erroneous longitudinal velocity estimate helps integrating the lateral velocity estimate in the right direction.

The deviation in lateral velocity in this period is probably due to a combination

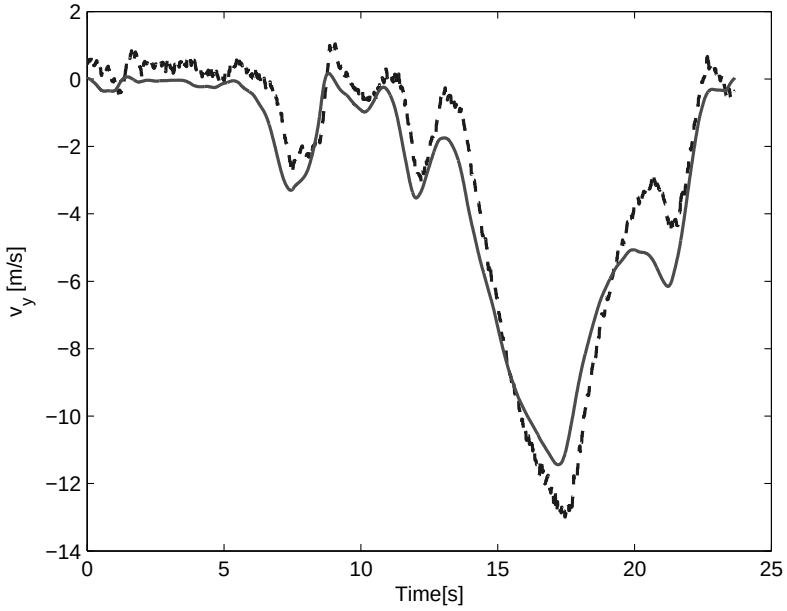

Figure 3.8: Estimate (solid) and measurement (dashed) of lateral velocity, circle on ice, modular observer.

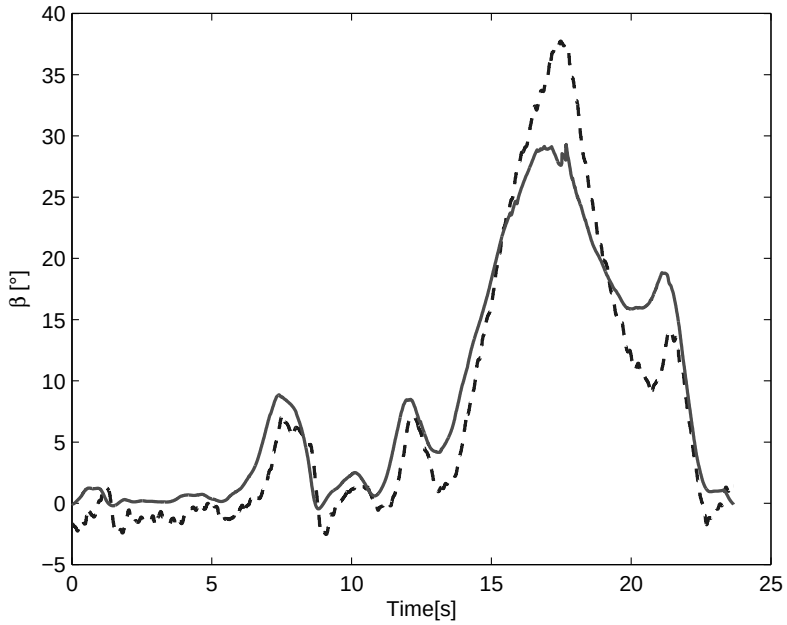

Figure 3.9: Estimate (solid) and measurement (dashed) of side slip, circle on ice, modular observer.

of

- less accurate friction model for large lateral slip values, and (more likely)
- the maximal friction coefficient changes: Inspection of the results indicates that the friction coefficient increases significantly after about 15 seconds, before it decreases again at around 18 seconds (in the same period, the ESP-flag is on). Setting the friction coefficient to 0.5 between 15 and 18 seconds gives significantly better estimates of lateral velocity (not shown here).

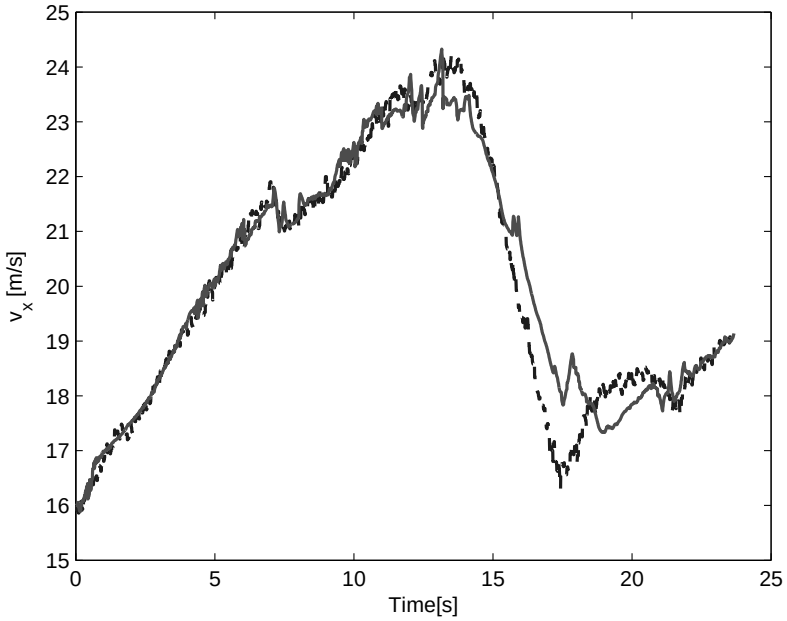

Figure 3.10: Estimate (solid) and measurement (dashed) of longitudinal velocity, circle on ice, full observer.

3.6.3 Verification of Assumption 2

As a verification of the main convergence assumption (Assumption 2), the condition (3.2) is calculated on basis of the friction model, using the velocity estimates and our guess of the maximal friction coefficient. The results are plotted in Figure 3.13 for both time series, and we see that the condition is always satisfied in both cases. The friction model used, is an in-house friction model of similar complexity to the magic formula tyre model. The complexity of calculating the condition using this friction model, is in the same order of magnitude as the complexity of the observer, which means that online convergence monitoring based on this condition should be computationally feasible.

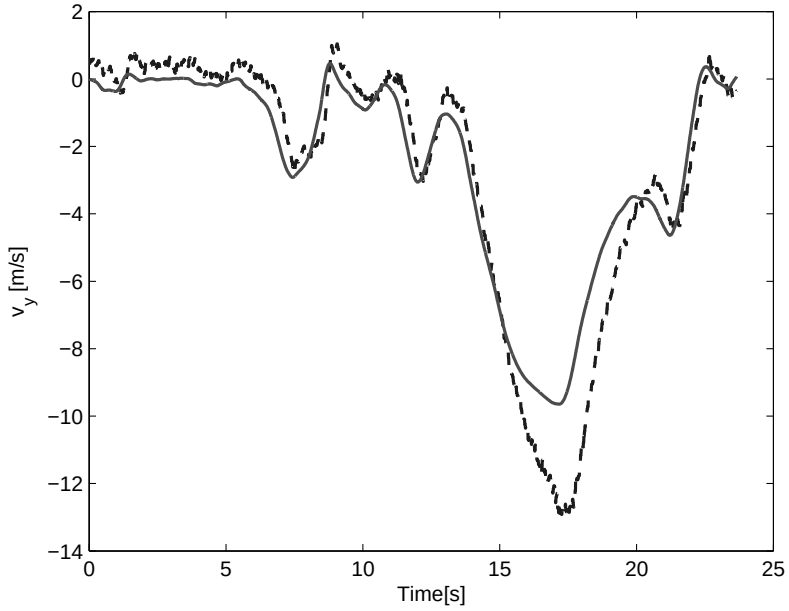

Figure 3.11: Estimate (solid) and measurement (dashed) of lateral velocity, circle on ice, full observer.

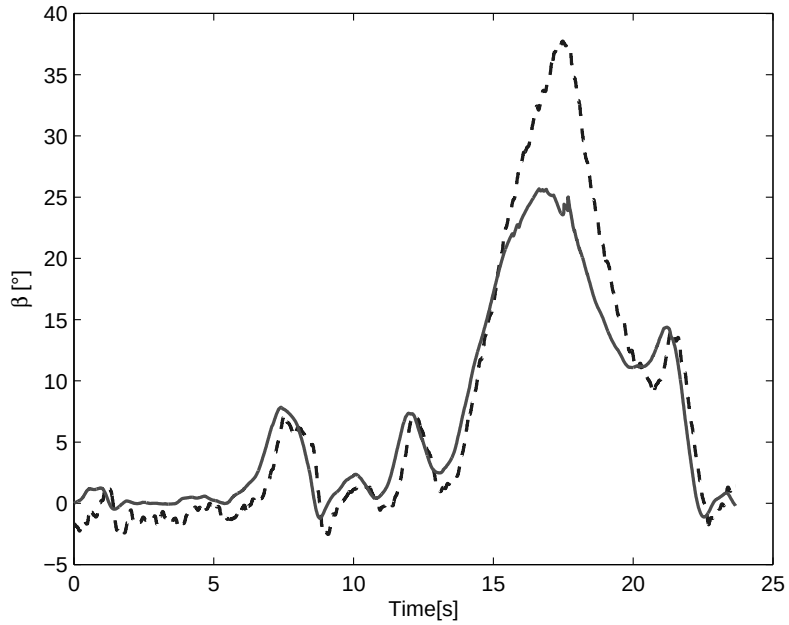

Figure 3.12: Estimate (solid) and measurement (dashed) of side slip, circle on ice, full observer.

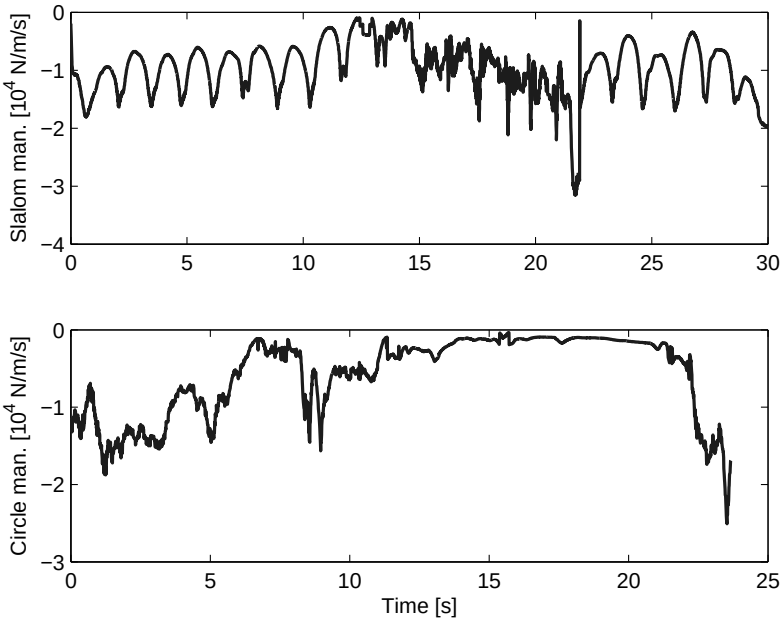

Figure 3.13: Condition (3.2) for slalom maneuver on asphalt, and circle maneuver on ice. The curves verify that Assumption 2 is always satisfied in these test drives.

3.7 Concluding remarks

Nonlinear observers for vehicle velocity and side-slip was proposed, which was proved to possess ISS-type stability properties under a certain condition on the friction model. The observer performs well when applied to experimental data from a car.

The main advantage of using nonlinear observers compared to the Extended Kalman Filter (EKF), is reduced computational complexity. While the number of ODEs to solve for an EKF is $3/2n+1/2n^2$, nonlinear observers usually have to solve n (the number of estimated variables) ODEs. In addition, for the EKF the nonlinear ODE (and/or measurement equation) have to be linearized at each sample, which along with monitoring of boundedness of the covariance matrix also might induce considerable computation.

The few tuning knobs of the observer simplifies tuning compared to tuning the covariance matrices of an EKF. For example, the observer of lateral velocity in the modular approach has only two tuning knobs, with some hints on how to tune given from the theoretical gain requirements.

A requirement for good performance of the observer, is information of maximal friction coefficient between tyre/road, in addition to information of road bank angle, and possibly inclination angle in the case of non-flat road. If the maximal friction coefficient is not known nor measured/estimated, the observer for lateral velocity in the modular approach can still be used if the longitudinal friction forces are measured, by calculating the lateral friction forces based on these, for instance as in [24].

Measurement errors such as bias in acceleration and yaw rate measurements, are

not considered herein. Such practical issues are important for observer performance.

Chapter 4

Preliminary velocity observer design with friction adaptation

The theory document describes a nonlinear adaptive observer for estimation of the velocities when the friction coefficients are unknown. *Lyapunov methods are used to derive a stable adaptation law for friction.*

4.1 Model

4.1.1 Car Dynamics

The car dynamics is written as [7]:

$$\dot{v}_x = v_y r + a_x^c \tag{4.1}$$

$$\dot{v}_y = -v_x r + a_y^c \tag{4.2}$$

$$\dot{r} = \frac{1}{J_z} \sum_{i=1}^{4} \mathbf{g}_i^\top \mathbf{R}(\delta_i) \mathbf{F}_i(t, \mathbf{x}, \theta_i) \tag{4.3}$$

where the nonlinear function $\mathbf{F}_i(t, \mathbf{x}, \theta_i)$ is defined as:

$$\mathbf{F}_i(t, \mathbf{x}, \theta_i) := \mathbf{F}'_i(\mathbf{x}, \theta_i, \delta_i, \omega_i) \tag{4.4}$$

since $\delta_i(t)$ and $\omega_i(t)$ are known, measured and bounded signals for all t.

4.2 Nonlinear Observer

4.2.1 Observer Dynamics

The observer equations are chosen as:

$$\dot{\hat{v}}_x = \hat{v}_y r + \sum_{i=1}^{4} K_i(a_x^c)(v_{x,i} - \hat{v}_x)$$

$$\dot{\hat{v}}_y = -\hat{v}_x r + a_y^c - K_{v_y} \sum_{i=1}^{4} \left(m a_y^s - [0,1]\mathbf{R}(\delta_i)\mathbf{F}_i(t,\hat{\mathbf{x}},\theta_i) \right)$$

$$\dot{\hat{r}} = \frac{1}{J_z} \sum_{i=1}^{4} \mathbf{g}_i^\top \mathbf{R}(\delta_i)\mathbf{F}_i(t,\hat{\mathbf{x}},\theta_i) + K_r \tilde{r}$$

where

$$m a_y^s = [0,1]\mathbf{R}(\delta_i)\mathbf{F}_i(t,\mathbf{x},\theta_i) \tag{4.5}$$

In this model we have assumed that the friction parameters θ_i are known. This assumption will be relaxed when designing the adaptive observer.

4.2.2 Error Dynamics

The error dynamics is:

$$\dot{\tilde{v}}_x = \tilde{v}_y r - \sum_{i=1}^{4} K_i(a_x^c)\tilde{v}_x + u \tag{4.6}$$

$$\dot{\tilde{v}}_y = -\tilde{v}_x r + K_{v_y} \sum_{i=1}^{4} [0,1]\mathbf{R}(\delta_i) \left(\mathbf{F}_i(t,\mathbf{x},\theta_i) - \mathbf{F}_i(t,\hat{\mathbf{x}},\theta_i) \right) \tag{4.7}$$

$$\dot{\tilde{r}} = \frac{1}{J_z} \sum_{i=1}^{4} \mathbf{g}_i^\top \mathbf{R}(\delta_i) \left(\mathbf{F}_i(t,\mathbf{x},\theta_i) - \mathbf{F}_i(t,\hat{\mathbf{x}},\theta_i) \right) - K_r \tilde{r} \tag{4.8}$$

4.3 Lyapunov-Based Adaptive Friction Estimator

The main goal for the adaptive friction estimator is to replace the friction parameter θ with an on-line estimate $\hat{\theta}$.

Assumption A1:
Assume that the equilibrium point $\chi = \mathbf{0}$ of the nominal system $\dot{\chi} = \mathbf{f}(t,\chi,\theta)$ is ULES. Hence,

$$V_1(t,\chi) = \frac{1}{2}\chi^\top \chi \tag{4.9}$$

is a Lyapunov function that satisfies:

$$c_1 \|\chi\|^2 \leq V_1(t,\chi) \leq c_2 \|\chi\|^2 \tag{4.10}$$

$$\frac{\partial V_1}{\partial t} + \frac{\partial V_1}{\partial \chi}\mathbf{f}(t,\chi,\theta) \leq -c_3 \|\chi\|^2 \tag{4.11}$$

$$\left\| \frac{\partial V_1}{\partial \chi} \right\| \leq c_4 \|\chi\| \tag{4.12}$$

In the fortcoming we will consider the following two parametrizations of the friction parameters:

4.3.1 Parametrization P1

The nonlinear function $\mathbf{F}_i(t,x,\theta_i)$ can be parametrized as a truncated Taylor-series expansion in θ_i such that:

$$\mathbf{F}_i(t,\mathbf{x},\theta_i) := \mathbf{F}_i(t,\mathbf{x},\hat{\theta}_i) + \left.\frac{\partial \mathbf{F}_i(t,\mathbf{x},\theta_i)}{\partial \theta_i}\right|_{\theta_i=\hat{\theta}_i} (\theta_i - \hat{\theta}_i) \tag{4.13}$$

or

$$\mathbf{F}_i(t,\mathbf{x},\theta_i) = \mathbf{F}_i(t,\mathbf{x},\hat{\theta}_i) + \mathbf{F}_{\theta_i}(t,\mathbf{x},\hat{\theta}_i)\tilde{\theta}_i \tag{4.14}$$

where $\tilde{\theta}_i = \theta_i - \hat{\theta}_i$ and:

$$\mathbf{F}_{\theta_i}(t,\mathbf{x},\hat{\theta}_i) = \left.\frac{\partial \mathbf{F}_i(t,\mathbf{x},\theta_i)}{\partial \theta_i}\right|_{\theta_i=\hat{\theta}_i} \tag{4.15}$$

This implies that:

$$\mathbf{F}_i(t,\hat{\mathbf{x}},\theta_i) = \mathbf{F}_i(t,\hat{\mathbf{x}},\hat{\theta}_i) + \mathbf{F}_{\theta_i}(t,\hat{\mathbf{x}},\hat{\theta}_i)\tilde{\theta}_i \tag{4.16}$$

Hence:

$$\begin{aligned}\mathbf{F}_i(t,\mathbf{x},\theta_i) - \mathbf{F}_i(t,\hat{\mathbf{x}},\theta_i) &= \mathbf{F}_i(t,\mathbf{x},\theta_i) - \left(\mathbf{F}_i(t,\hat{\mathbf{x}},\hat{\theta}_i) + \mathbf{F}_{\theta_i}(t,\hat{\mathbf{x}},\hat{\theta}_i)\tilde{\theta}_i\right) \\ &= \mathbf{F}_i(t,\mathbf{x},\theta_i) - \mathbf{F}_i(t,\hat{\mathbf{x}},\hat{\theta}_i) - \mathbf{F}_{\theta_i}(t,\hat{\mathbf{x}},\hat{\theta}_i)\tilde{\theta}_i \end{aligned} \tag{4.17}$$

This can be written

$$\mathbf{F}_i(t,\mathbf{x},\theta_i) - \mathbf{F}_i(t,\hat{\mathbf{x}},\hat{\theta}_i) = \tilde{\mathbf{F}}_i(t,\mathbf{x},\hat{\mathbf{x}},\theta_i) + \mathbf{F}_{\theta_i}(t,\hat{\mathbf{x}},\hat{\theta}_i)\tilde{\theta}_i \tag{4.18}$$

where:

$$\tilde{\mathbf{F}}_i(t,\mathbf{x},\hat{\mathbf{x}},\theta_i) = \mathbf{F}_i(t,\mathbf{x},\theta_i) - \mathbf{F}_i(t,\hat{\mathbf{x}},\theta_i) \tag{4.19}$$

In the adaptive case (4.18) is substituted into the error dynamics (4.6)–(4.8). This gives one additional term due to $\mathbf{F}_{\theta_i}(t,\hat{\mathbf{x}},\hat{\theta}_i)\tilde{\theta}_i$ which can be overparametrized in the friction parameters by using the following regressor models:

$$K_{v_y} \sum_{i=1}^{4} [0,1]\mathbf{R}(\delta_i)\mathbf{F}_{\theta_i}(t,\hat{\mathbf{x}},\hat{\theta}_i)\tilde{\theta}_i := \phi_{v_y}^{\top}(t,\hat{\mathbf{x}},\hat{\theta}_{v_y})\tilde{\theta}_{v_y} \tag{4.20}$$

$$\frac{1}{J_z}\sum_{i=1}^{4} \mathbf{g}_i^{\top}\mathbf{R}(\delta_i)\mathbf{F}_{\theta_{i+4}}(t,\hat{\mathbf{x}},\hat{\theta}_{i+4})\tilde{\theta}_{i+4} := \phi_r^{\top}(t,\hat{\mathbf{x}},\hat{\theta}_r)\tilde{\theta}_r \tag{4.21}$$

where $\tilde{\theta}_{v_y} \in \mathbb{R}^4$ and $\tilde{\theta}_r \in \mathbb{R}^4$ are the friction parameter errors:

$$\tilde{\theta}_{v_y} = [\tilde{\theta}_1, \tilde{\theta}_2, \tilde{\theta}_3, \tilde{\theta}_4]^\top \tag{4.22}$$

$$\tilde{\theta}_r = [\tilde{\theta}_5, \tilde{\theta}_6, \tilde{\theta}_7, \tilde{\theta}_8]^\top \tag{4.23}$$

The corresponding regressor vectors $\phi_{v_y}(t, \hat{x}, \hat{\theta}_{v_y}) \in \mathbb{R}^{4\times 1}$ and $\phi_r(t, \hat{x}, \hat{\theta}_r) \in \mathbb{R}^{4\times 1}$ are:

$$\phi_{v_y}^\top(t, \hat{\mathbf{x}}, \hat{\theta}) = \begin{bmatrix} K_{v_y}[0,1]\mathbf{R}(\delta_1)\mathbf{F}_{\theta_1} & K_{v_y}[0,1]\mathbf{R}(\delta_2)\mathbf{F}_{\theta_2} & K_{v_y}[0,1]\mathbf{R}(\delta_3)\mathbf{F}_{\theta_3} & K_{v_y}[0,1]\mathbf{R}(\delta_4)\mathbf{F}_{\theta_4} \end{bmatrix}$$

$$\phi_r^\top(t, \hat{\mathbf{x}}, \hat{\theta}) = \begin{bmatrix} \frac{1}{J_z}\mathbf{g}_1^\top\mathbf{R}(\delta_1)\mathbf{F}_{\theta_5} & \frac{1}{J_z}\mathbf{g}_2^\top\mathbf{R}(\delta_2)\mathbf{F}_{\theta_6} & \frac{1}{J_z}\mathbf{g}_3^\top\mathbf{R}(\delta_3)\mathbf{F}_{\theta_7} & \frac{1}{J_z}\mathbf{g}_4^\top\mathbf{R}(\delta_4)\mathbf{F}_{\theta_8} \end{bmatrix}$$

The overparametrization is not critical since the main goal is to obtain convergence of the state estimates whereas the parameters are only used as additional states in order to achieve this.

An simplification could be to use one friction parameter for all the wheels implying that only two parameters are needed.

4.3.2 Parametrization P2

The nonlinear function $\mathbf{F}_i(t, x, \theta_i)$ can also be parametrized as a linear function in the friction parameter θ_i such that:

$$\mathbf{F}_i(t, \mathbf{x}, \theta_i) := \mathbf{A}_i(t, \mathbf{x})\theta_i \tag{4.24}$$

where is $\mathbf{A}_i(t, \mathbf{x})$ is the function $\mathbf{F}_i(t, x, \theta_i)$ evaluated at the nominal value $\theta_i = 1$. Moreover:

$$\mathbf{A}_i(t, \mathbf{x}) := \mathbf{F}_i(t, x, 1) \tag{4.25}$$

This suggests that:

$$\mathbf{F}_i(t, \hat{\mathbf{x}}, \theta_i) = \mathbf{A}_i(t, \hat{\mathbf{x}})\hat{\theta}_i + \mathbf{A}_i(t, \hat{\mathbf{x}})\tilde{\theta}_i \tag{4.26}$$

Hence, the error term becomes:

$$\begin{aligned} \mathbf{F}_i(t, \mathbf{x}, \theta_i) - \mathbf{F}_i(t, \hat{\mathbf{x}}, \theta_i) &= \mathbf{A}_i(t, \mathbf{x})\theta_i - \left(\mathbf{A}_i(t, \hat{\mathbf{x}})\hat{\theta}_i + \mathbf{A}_i(t, \hat{\mathbf{x}})\tilde{\theta}_i\right) \\ &= \mathbf{A}_i(t, \mathbf{x})\theta_i - \mathbf{A}_i(t, \hat{\mathbf{x}})\hat{\theta}_i - \mathbf{A}_i(t, \hat{\mathbf{x}})\tilde{\theta}_i \\ &= \mathbf{F}_i(t, \mathbf{x}, \theta_i) - \mathbf{F}_i(t, \hat{\mathbf{x}}, \hat{\theta}_i) - \mathbf{A}_i(t, \hat{\mathbf{x}})\tilde{\theta}_i \end{aligned} \tag{4.27}$$

or

$$\mathbf{F}_i(t, \mathbf{x}, \theta_i) - \mathbf{F}_i(t, \hat{\mathbf{x}}, \hat{\theta}_i) = \tilde{\mathbf{F}}_i(t, \mathbf{x}, \hat{\mathbf{x}}, \theta_i) + \mathbf{A}_i(t, \hat{\mathbf{x}})\tilde{\theta}_i \tag{4.28}$$

Then

$$K_{v_y} \sum_{i=1}^{4} [0,1]\mathbf{R}(\delta_i)\mathbf{A}_i(t, \hat{\mathbf{x}})\tilde{\theta}_i := \phi_{v_y}^\top(t, \hat{\mathbf{x}}, \hat{\theta}_{v_y})\tilde{\theta}_{v_y} \tag{4.29}$$

$$\frac{1}{J_z} \sum_{i=1}^{4} \mathbf{g}_i^\top \mathbf{R}(\delta_i)\mathbf{A}_i(t, \hat{\mathbf{x}})\tilde{\theta}_{i+4} := \phi_r^\top(t, \hat{\mathbf{x}}, \hat{\theta}_r)\tilde{\theta}_r \tag{4.30}$$

where $\tilde{\theta}_{v_y} \in \mathbb{R}^4$ and $\tilde{\theta}_r \in \mathbb{R}^4$ are the friction parameter errors:

$$\tilde{\theta}_{v_y} = [\tilde{\theta}_1, \tilde{\theta}_2, \tilde{\theta}_3, \tilde{\theta}_4]^\top \tag{4.31}$$

$$\tilde{\theta}_r = [\tilde{\theta}_5, \tilde{\theta}_6, \tilde{\theta}_7, \tilde{\theta}_8]^\top \tag{4.32}$$

The corresponding regressor vectors $\phi_{v_y}(t, \hat{x}, \hat{\theta}_{v_y}) \in \mathbb{R}^{4\times 1}$ and $\phi_r(t, \hat{x}, \hat{\theta}_r) \in \mathbb{R}^{4\times 1}$ are:

$$\phi_{v_y}^\top(t, \hat{\mathbf{x}}, \hat{\theta}) = \left[K_{v_y}[0,1]\mathbf{R}(\delta_1)\mathbf{A}_1 \;\; K_{v_y}[0,1]\mathbf{R}(\delta_2)\mathbf{A}_2 \;\; K_{v_y}[0,1]\mathbf{R}(\delta_3)\mathbf{A}_3 \;\; K_{v_y}[0,1]\mathbf{R}(\delta_4)\mathbf{A}_4 \right]$$

$$\phi_r^\top(t, \hat{\mathbf{x}}, \hat{\theta}) = \left[\;\; \tfrac{1}{J_z}\mathbf{g}_1^\top\mathbf{R}(\delta_1)\mathbf{A}_1 \quad \tfrac{1}{J_z}\mathbf{g}_2^\top\mathbf{R}(\delta_2)\mathbf{A}_2 \quad \tfrac{1}{J_z}\mathbf{g}_3^\top\mathbf{R}(\delta_3)\mathbf{A}_3 \quad \tfrac{1}{J_z}\mathbf{g}_4^\top\mathbf{R}(\delta_4)\mathbf{A}_4 \;\; \right]$$

An simplification could be to use one friction parameter for all the wheels implying that only two parameters are needed.

4.3.3 Error Dynamics for the Adaptive Observer

Choosing:

$$\dot{\hat{v}}_x = \hat{v}_y r + \sum_{i=1}^{4} K_i(a_x^c)(v_{x,i} - \hat{v}_x)$$

$$\dot{\hat{v}}_y = -\hat{v}_x r + a_y^c - K_{v_y} \sum_{i=1}^{4} \left(m a_y^s - [0,1]\mathbf{R}(\delta_i)\mathbf{F}(t, \hat{\mathbf{x}}_i, \hat{\theta}_i) \right)$$

$$\dot{\hat{r}} = \frac{1}{J_z} \sum_{i=1}^{4} \mathbf{g}_i^\top \mathbf{R}(\delta_i)\mathbf{F}(t, \hat{\mathbf{x}}_i, \hat{\theta}_{i+4}) + K_r \tilde{r}$$

where we have replaced θ with the adaptive estimate $\hat{\theta}$ in the lateral and yaw equations. This gives the error dynamics:

$$\dot{\tilde{v}}_x = \tilde{v}_y r - \sum_{i=1}^{4} K_i(a_x^c)\tilde{v}_x + u \tag{4.33}$$

$$\dot{\tilde{v}}_y = -\tilde{v}_x r + K_{v_y} \sum_{i=1}^{4} [0,1]\mathbf{R}(\delta_i) \left(\mathbf{F}_i(t, \mathbf{x}, \theta_i) - \mathbf{F}(t, \hat{\mathbf{x}}, \hat{\theta}_i) \right) \tag{4.34}$$

$$\dot{\tilde{r}} = \frac{1}{J_z} \sum_{i=1}^{4} \mathbf{g}_i^\top \mathbf{R}(\delta_i) \left(\mathbf{F}_i(t, \mathbf{x}, \theta_{i+4}) - \mathbf{F}_i(t, \hat{\mathbf{x}}, \hat{\theta}_{i+4}) \right) - K_r \tilde{r} \tag{4.35}$$

From Parametrizations P1 and P2 we have the following expression for the error terms:

$$\mathbf{F}_i(t, \mathbf{x}, \theta_i) - \mathbf{F}_i(t, \hat{\mathbf{x}}, \hat{\theta}_i) = \tilde{\mathbf{F}}_i(t, \mathbf{x}, \hat{\mathbf{x}}, \theta_i) + \mathbf{F}_{\theta_i}(t, \hat{\mathbf{x}}, \hat{\theta}_i)\tilde{\theta}_i \tag{4.36}$$

$$\mathbf{F}_i(t, \mathbf{x}, \theta_i) - \mathbf{F}_i(t, \hat{\mathbf{x}}, \hat{\theta}_i) = \tilde{\mathbf{F}}_i(t, \mathbf{x}, \hat{\mathbf{x}}, \theta_i) + \mathbf{A}_i(t, \hat{\mathbf{x}})\tilde{\theta}_i \tag{4.37}$$

This gives:

$$\dot{\tilde{v}}_x = \tilde{v}_y r - \sum_{i=1}^{4} K_i(a_x^c)\tilde{v}_x + u$$

$$\dot{\tilde{v}}_y = -\tilde{v}_x r + K_{v_y} \sum_{i=1}^{4} [0,1]\mathbf{R}(\delta_i)\tilde{\mathbf{F}}_i(t,\mathbf{x},\hat{\mathbf{x}},\theta_i) + \phi_{v_y}^{\top}(t,\hat{\mathbf{x}},\hat{\theta}_{v_y})\tilde{\theta}_{v_y}$$

$$\dot{\tilde{r}} = \frac{1}{J_z}\sum_{i=1}^{4} \mathbf{g}_i^{\top}\mathbf{R}(\delta_i)\tilde{\mathbf{F}}_i(t,\mathbf{x},\hat{\mathbf{x}},\theta_{i+4}) - K_r\tilde{r} + \phi_r^{\top}(t,\hat{\mathbf{x}},\hat{\theta}_r)\tilde{\theta}_r$$

This system can be compactly written as:

$$\dot{\chi} = \mathbf{f}(t,\chi,\theta) + \mathbf{B}\mathbf{\Phi}(t,\hat{\mathbf{x}},\hat{\theta})\tilde{\theta} + \mathbf{w}$$

where

$$\mathbf{f}(t,\chi,\theta) = \begin{bmatrix} \tilde{v}_y r - \sum_i K_i(a_x^c)\tilde{v}_x \\ -\tilde{v}_x r + K_{v_y}\sum_i [0,1]\mathbf{R}(\delta_i)\tilde{\mathbf{F}}_i(t,\mathbf{x},\hat{\mathbf{x}},\theta_i) \\ \frac{1}{J_z}\sum_i \mathbf{g}_i^{\top}\mathbf{R}(\delta_i)\tilde{\mathbf{F}}_i(t,\mathbf{x},\hat{\mathbf{x}},\theta_i) - K_r\tilde{r} \end{bmatrix} \tag{4.38}$$

$$\mathbf{B} = \begin{bmatrix} 0 & 0 \\ 1 & 0 \\ 0 & 1 \end{bmatrix} \tag{4.39}$$

$$\mathbf{\Phi}(t,\hat{\mathbf{x}},\hat{\theta}) = \begin{bmatrix} \phi_{v_y}^{\top}(t,\hat{\mathbf{x}},\hat{\theta}_{v_y}) & \mathbf{0}_{1\times 4} \\ \mathbf{0}_{1\times 4} & \phi_r^{\top}(t,\hat{\mathbf{x}},\hat{\theta}_r) \end{bmatrix} \tag{4.40}$$

$$\tilde{\theta} = \begin{bmatrix} \tilde{\theta}_{v_y}^{\top}, \tilde{\theta}_r^{\top} \end{bmatrix} \tag{4.41}$$

$$\mathbf{w} = \begin{bmatrix} u \\ 0 \\ 0 \end{bmatrix} \tag{4.42}$$

4.3.4 Lyapunov Analysis

In the Lyapunov analysis we will assume:
Assumption A2:
The forward speed v_x is known.

Assumption A3:
The estimator error system is forward complete in $\delta_i(t)$ and $r(t)$, that is the solutions of the ODEs exist for all $\delta_i(t)$ and $r(t)$.

Consider the quadratic Lyapunov function candidate:

$$V = \frac{1}{2}\chi^{\top}\chi + \frac{1}{2}\tilde{\theta}_{v_y}^{\top}\Gamma_{v_y}^{-1}\tilde{\theta}_{v_y} + \frac{1}{2}\tilde{\theta}_r^{\top}\Gamma_r^{-1}\tilde{\theta}_r \tag{4.43}$$

This gives

$$\begin{aligned}\dot{V} &= \chi^{\top}\mathbf{f}(t,\chi,\theta) + \tilde{v}_y\left(\phi_{v_y}^{\top}(t,\hat{\mathbf{x}},\hat{\theta}_{v_y})\tilde{\theta}_{v_y}\right) + \tilde{r}\left(\phi_r^{\top}(t,\hat{\mathbf{x}},\hat{\theta}_r)\tilde{\theta}_r\right) + \tilde{\theta}_{v_y}^{\top}\Gamma_{v_y}^{-1}\dot{\tilde{\theta}}_{v_y} + \tilde{\theta}_r^{\top}\Gamma_r^{-1}\dot{\tilde{\theta}}_r \\ &= \chi^{\top}\mathbf{f}(t,\chi,\theta) + \tilde{\theta}_{v_y}^{\top}\left(\Gamma_{v_y}^{-1}\dot{\tilde{\theta}}_{v_y} + \phi_{v_y}(t,\hat{\mathbf{x}},\hat{\theta}_{v_y})\tilde{v}_y\right) + \tilde{\theta}_r^{\top}\left(\Gamma_r^{-1}\dot{\tilde{\theta}}_r + \phi_r(t,\hat{\mathbf{x}},\hat{\theta}_r)\tilde{r}\right)\end{aligned}$$

The error terms $\tilde{v}_y$ is given by the following ODE:

$$\dot{\tilde{v}}_y = K_{v_y} \sum_{i=1}^{4} [0,1]\mathbf{R}(\delta_i)\tilde{\mathbf{F}}_i(t,\mathbf{x},\hat{\mathbf{x}},\theta_i) + \phi_{v_y}^{\top}(t,\hat{\mathbf{x}},\hat{\theta}_{v_y})\tilde{\theta}_{v_y} \tag{4.44}$$

The term $z = \tilde{v}_y$ can also be computed using the friction model:

$$\dot{z} = K_{v_y} \sum_{i=1}^{4} \left(ma_y^s - [0,1]\mathbf{R}(\delta_i)\mathbf{F}_i(t,\hat{\mathbf{x}},\hat{\theta}_i) \right), \qquad z(0) = 0 \tag{4.45}$$

where we have introduced the new state variable z to distinguish the solutions (4.44) and (4.45). The initial value of z must, however, be chosen as zero corresponding to zero lateral velocity $\tilde{v}_y$ since $v_y(0)$ is unknown (unmeasured). This implies that the observer must be started when the car is at rest.

Choosing the adaptive laws as:

$$\dot{\hat{\theta}}_{v_y} = -\Gamma_{v_y}\phi_{v_y}(t,\hat{\mathbf{x}},\hat{\theta}_{v_y})z \tag{4.46}$$

$$\dot{\hat{\theta}}_r = -\Gamma_r\phi_r(t,\hat{\mathbf{x}},\hat{\theta}_r)\tilde{r} \tag{4.47}$$

finally gives

$$\dot{V} = \dot{V}_1 \leq 0 \tag{4.48}$$

by Assumption A1. Then by standard *Lyapunov analysis* the adaptive observer is convergent and $\hat{\chi} \to \chi$ whereas $\tilde{\theta}_{v_y}$ and $\tilde{\theta}_r$ are bounded. It also follows from standard arguments that PE guarantees asymptotic stability (*Matrosov's theorem*), that is $\tilde{r} \to 0, \tilde{v}_y \to 0, \tilde{\theta}_{v_y} \to \mathbf{0}$, and $\tilde{\theta}_r \to \mathbf{0}$ if system is PE. The requirements for Parametrizations P1 and P2 are:

$$\int_t^{t+T} \phi_{v_y}(t,\hat{\mathbf{x}},\hat{\theta}_{v_y})\phi_{v_y}^{\top}(t,\hat{\mathbf{x}},\hat{\theta}_{v_y})dt$$
$$= \sum_{i=1}^{4} \left(\mathbf{F}_{\theta_i}^{\top}(t,\hat{\mathbf{x}},\hat{\theta}_{v_y})\mathbf{R}^{\top}(\delta_i) \begin{bmatrix} 0 \\ 1 \end{bmatrix} \right) \left(\mathbf{F}_{\theta_i}^{\top}(t,\hat{\mathbf{x}},\hat{\theta}_{v_y})\mathbf{R}^{\top}(\delta_i) \begin{bmatrix} 0 \\ 1 \end{bmatrix} \right)^{\top} dt \geq \mu_1$$

$$\int_t^{t+T} \phi_r(t,\hat{\mathbf{x}},\hat{\theta}_r)\phi_r^{\top}(t,\hat{\mathbf{x}},\hat{\theta}_r)dt$$
$$= \int_t^{t+T} \left(\sum_{i=1}^{4} \mathbf{F}_{\theta_{i+4}}^{\top}(t,\hat{\mathbf{x}},\hat{\theta}_r)\mathbf{R}^{\top}(\delta_i)\mathbf{g}_i \right) \left(\sum_{i=1}^{4} \mathbf{F}_{\theta_{i+4}}^{\top}(t,\hat{\mathbf{x}},\hat{\theta}_r)\mathbf{R}^{\top}(\delta_i)\mathbf{g}_i \right)^{\top} dt \geq \mu_2$$

and

$$\int_t^{t+T} \phi_{v_y}(t,\hat{\mathbf{x}},\hat{\theta}_{v_y})\phi_{v_y}^{\top}(t,\hat{\mathbf{x}},\hat{\theta}_{v_y})dt$$
$$= \sum_{i=1}^{4} \left(\mathbf{A}_i^{\top}(t,\hat{\mathbf{x}})\mathbf{R}^{\top}(\delta_i) \begin{bmatrix} 0 \\ 1 \end{bmatrix} \right) \left(\mathbf{A}_i^{\top}(t,\hat{\mathbf{x}})\mathbf{R}^{\top}(\delta_i) \begin{bmatrix} 0 \\ 1 \end{bmatrix} \right)^{\top} dt \geq \mu_1$$

$$\int_t^{t+T} \phi_r(t,\hat{\mathbf{x}},\hat{\theta}_r)\phi_r^\top(t,\hat{\mathbf{x}},\hat{\theta}_r)dt$$
$$= \int_t^{t+T} \left(\sum_{i=1}^4 \mathbf{A}_i^\top(t,\hat{\mathbf{x}})\mathbf{R}^\top(\delta_i)\mathbf{g}_i\right)\left(\sum_{i=1}^4 \mathbf{A}_i^\top(t,\hat{\mathbf{x}})\mathbf{R}^\top(\delta_i)\mathbf{g}_i\right)^\top dt \geq \mu_2$$

4.4 Robustification Schemes

The adaptive laws in the previous section are based on a plant model that is free of noise, disturbances and unmodeled dynamics. The proposed schemes will be implemented on an actual car that most likely deviate from the plant model on which the design is based. In this section we propose several techniques to modify the adaptive scheme and establish robustness with respect to bounded disturbances and unmodeled dynamics.

4.4.1 Unknown Bounded Disturbances

It is well known that external disturbances may cause parameter drift. Assume that *unknown bounded disturbances* d_y and d_r enters the error dynamics according to:

$$\dot{\tilde{v}}_y = K_{v_y}\sum_{i=1}^4 [0,1]\mathbf{R}(\delta_i)\tilde{\mathbf{F}}_i(t,\mathbf{x},\hat{\mathbf{x}},\theta_i) + \phi_{v_y}^\top(t,\hat{\mathbf{x}},\hat{\theta}_{v_y})\tilde{\theta}_{v_y} + d_y \tag{4.49}$$

$$\dot{\tilde{r}} = \frac{1}{J_z}\sum_{i=1}^4 \mathbf{g}_i^\top\mathbf{R}(\delta_i)\tilde{\mathbf{F}}_i(t,\mathbf{x},\hat{\mathbf{x}},\theta_{i+4}) - K_r\tilde{r} + \phi_r^\top(t,\hat{\mathbf{x}},\hat{\theta}_r)\tilde{\theta}_r + d_r \tag{4.50}$$

These terms will propagate to the Lyapunov function according to:

$$\dot{V} = \chi^\top\mathbf{f}(t,\chi,\theta) + \tilde{v}_y\left(\phi_{v_y}^\top(t,\hat{\mathbf{x}},\hat{\theta}_{v_y})\tilde{\theta}_{v_y} + d_y\right) + \tilde{r}\left(\phi_r^\top(t,\hat{\mathbf{x}},\hat{\theta}_r)\tilde{\theta}_r + d_r\right) + \tilde{\theta}_{v_y}^\top\Gamma_{v_y}^{-1}\dot{\tilde{\theta}}_{v_y} + \tilde{\theta}_r^\top\Gamma_r^{-1}\dot{\tilde{\theta}}_r$$
$$= \chi^\top\mathbf{f}(t,\chi,\theta) + \tilde{\theta}_{v_y}^\top\left(\Gamma_{v_y}^{-1}\dot{\tilde{\theta}}_{v_y} + \phi_{v_y}(t,\hat{\mathbf{x}},\hat{\theta}_{v_y})\tilde{v}_y\right) + \tilde{\theta}_r^\top\left(\Gamma_r^{-1}\dot{\tilde{\theta}}_r + \phi_r(t,\hat{\mathbf{x}},\hat{\theta}_r)\tilde{r}\right) + \tilde{v}_y d_y + \tilde{r}d_r$$

If the adaptive laws are chosen as (4.46)–(4.47) this results in:

$$\dot{V} = \chi^\top\mathbf{f}(t,\chi,\theta) + \tilde{v}_y d_y + \tilde{r}d_r \tag{4.51}$$

Hence, the parameter adaptation law will be will be sensitive to the time-varying noise term since the error terms $\tilde{v}_y$ and $\tilde{r}$ are driven by d_y and d_r. However, precautions for bounded disturbances can be taken by modifying the adaptation laws. We will discuss several methods for this:

4.4.2 Dead-Zone Technique (Bound on Disturbances)

Peterson and Narendra [18] propose stopping the adaptation when the output errors (z, $\tilde{r}$) become smaller than prescribed values (Δ_y, Δ_r) by introducing a dead-zone in the adaptation law. This is due the fact that small tracking errors mainly contain

noise and disturbances. This suggests that:

$$\dot{\hat{\theta}}_{v_y} = \begin{cases} -\Gamma_{v_y}\phi_{v_y}(t,\hat{\mathbf{x}},\hat{\theta}_{v_y})z & |z| \geq \Delta_y \\ \mathbf{0} & |z| < \Delta_y \end{cases}$$
$$\dot{\hat{\theta}}_{r} = \begin{cases} -\Gamma_{r}\phi_{r}(t,\hat{\mathbf{x}},\hat{\theta}_{r})\tilde{r} & |\tilde{v}_r| \geq \Delta_r \\ \mathbf{0} & |\tilde{v}_r| < \Delta_r \end{cases}$$

Hence, by choosing (Δ_y, Δ_r) sufficient large $\dot{V}$ becomes non-increasing outside the dead zone. The choice $\dot{\tilde{\theta}}_{v_y} = \mathbf{0}$ and $\dot{\tilde{\theta}}_r = \mathbf{0}$ inside the dead-zone implies that the cancellation of the error terms $\tilde{\theta}_{v_y}$ and $\tilde{\theta}_r$ in $\dot{V}$ no longer is satisfied. As a result of this, $\dot{V}$ may grow inside the dead-zone. Hence, asymptotic convergence of the plant output to the desired trajectory no longer can be guaranteed even when no disturbances are present.

The choice of (Δ_y, Δ_r) should be seen as a trade-off between robustness and performance. A large value for implies that the parameter adaptation is less sensitive for plant disturbances while a low yields better performance but increased possibility for parameter drift. Still, mainly because of its simplicity and effectiveness, this method is highly attractive to use.

4.4.3 Bound on the Parameters

If bounds on the desired parameter vector are known, instability due to parameter errors can be avoided by a straightforward modification of the adaptive law. This problem has been addressed by Kresselmeier and Narendra [14] for instance. They assume that bounds $(\theta_{y,\max}, \theta_{r,\max})$ on the parameter vectors are known such that:

$$\left\|\tilde{\theta}_{v_y}\right\| \leq \theta_{y,\max}, \qquad 0 < \theta_{y,\max} < \infty \tag{4.52}$$
$$\left\|\tilde{\theta}_{r}\right\| \leq \theta_{r,\max}, \qquad 0 < \theta_{r,\max} < \infty \tag{4.53}$$

The adaptive law is modified as:

$$\dot{\hat{\theta}}_{v_y} = -\Gamma_{v_y}\phi_{v_y}(t,\hat{\mathbf{x}},\hat{\theta}_{v_y})z - \hat{\theta}_{v_y}\left(1 - \frac{\left\|\hat{\theta}_{v_y}\right\|}{\theta_{y,\max}}\right)^2 f(\hat{\theta}_{v_y}, \theta_{y,\max})$$
$$\dot{\hat{\theta}}_{r} = -\Gamma_{r}\phi_{r}(t,\hat{\mathbf{x}},\hat{\theta}_{r})\tilde{r} - \hat{\theta}_{r}\left(1 - \frac{\left\|\hat{\theta}_{r}\right\|}{\theta_{r,\max}}\right)^2 f(\hat{\theta}_{r}, \theta_{r,\max})$$

where

$$f(\alpha,\alpha_{\max}) = \begin{cases} 1 & \text{if } \|\alpha\| > \alpha_{\max} \\ 0 & \text{otherwise} \end{cases}$$

4.4.4 Sigma Modification Schemes

The two previous schemes assume that a bound on the disturbance vector or the parameter vector is known. A popular robust adaptive control scheme where this a

priori information is not necessary was proposed by Ioannou and Kokotovic [9]. This scheme is usually referred to as the σ-modification scheme. To avoid the parameters growing unbounded in the presence of bounded disturbances additional stabilizing terms

$$\begin{aligned} &- \sigma_y \hat{\theta}_{v_y} \\ &- \sigma_r \hat{\theta}_r \end{aligned}$$

with $\sigma_y > 0$ and $\sigma_r > 0$ can be used in the adaptive laws. Hence:

$$\begin{aligned} \dot{\hat{\theta}}_{v_y} &= -\Gamma_{v_y} \phi_{v_y}(t, \hat{\mathbf{x}}, \hat{\theta}_{v_y}) z - \sigma_y \hat{\theta}_{v_y} \\ \dot{\hat{\theta}}_r &= -\Gamma_r \phi_r(t, \hat{\mathbf{x}}, \hat{\theta}_r) \tilde{r} - \sigma_r \hat{\theta}_r \end{aligned}$$

However, introduction of the terms $-\sigma_y \hat{\theta}_{v_y}$ and $-\sigma_r \hat{\theta}_r$ implies that the origin is no longer the equilibrium point. This implies that the parameter estimates will not converge to their true values even for a PE reference input or the case when all external disturbances are removed. To overcome the limitations of the σ-modification scheme Narendra and Annaswamy [16] proposed a slight modification of the above scheme, that is:

$$\begin{aligned} \dot{\hat{\theta}}_{v_y} &= -\Gamma_{v_y} \phi_{v_y}(t, \hat{\mathbf{x}}, \hat{\theta}_{v_y}) z - \sigma_y \left\| z \right\| \hat{\theta}_{v_y} \\ \dot{\hat{\theta}}_r &= -\Gamma_r \phi_r(t, \hat{\mathbf{x}}, \hat{\theta}_r) \tilde{r} - \sigma_r \left\| \tilde{r} \right\| \hat{\theta}_r \end{aligned}$$

The motivation for using the gains $\sigma_y \left\| z \right\|$ and $\sigma_r \left\| \tilde{r} \right\|$ instead is that this proportional term tends to zero with the tracking errors $\left\| z \right\|$ and $\left\| \tilde{r} \right\|$. Hence, parameter convergence to the true parameter values under the assumption of PE can be obtained when there are no external disturbances present.

A more detailed discussion on convergence properties, stability and implementation considerations are found in Narendra and Annaswamy [16]. This text also includes stability proofs for the above mentioned schemes.

4.5 Experimental Results

Some preliminary experimental results are presented below. A parametrization where two friction coefficients are adapted, one for lateral velocity and one for yaw rate. Figures 4.1-4.5 are for the slalom maneuver case in the previous chapter, where the friction coefficient is high (dry asphalt). Figures 4.6-4.10 are for the circle on ice maneuver, with a low friction coefficient.

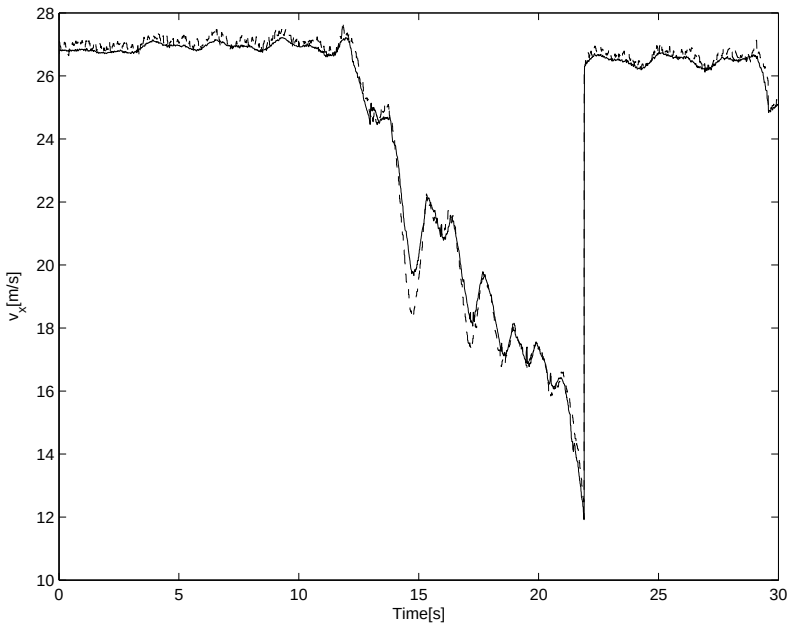

Figure 4.1: Estimate (solid) and measurement (dashed) of longitudinal velocity, high friction coefficient.

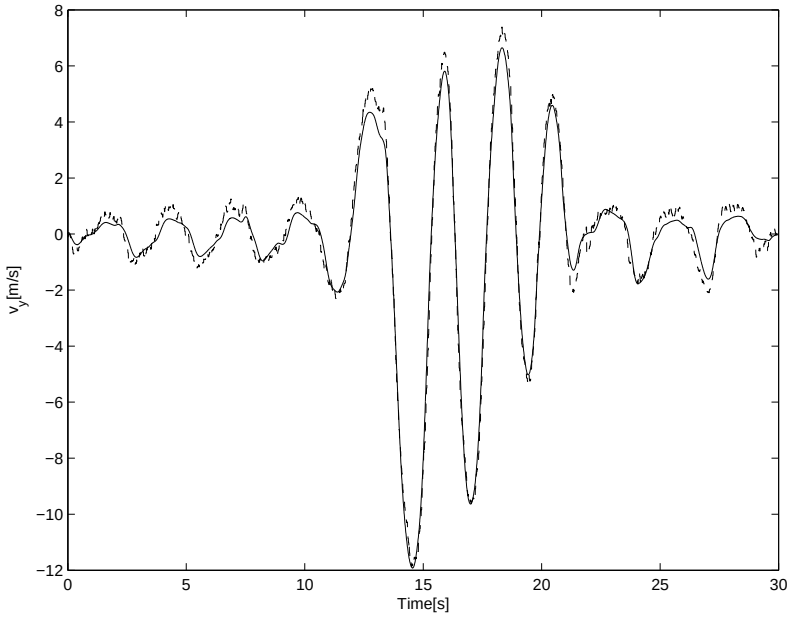

Figure 4.2: Estimate (solid) and measurement (dashed) of lateral velocity, high friction coefficient.

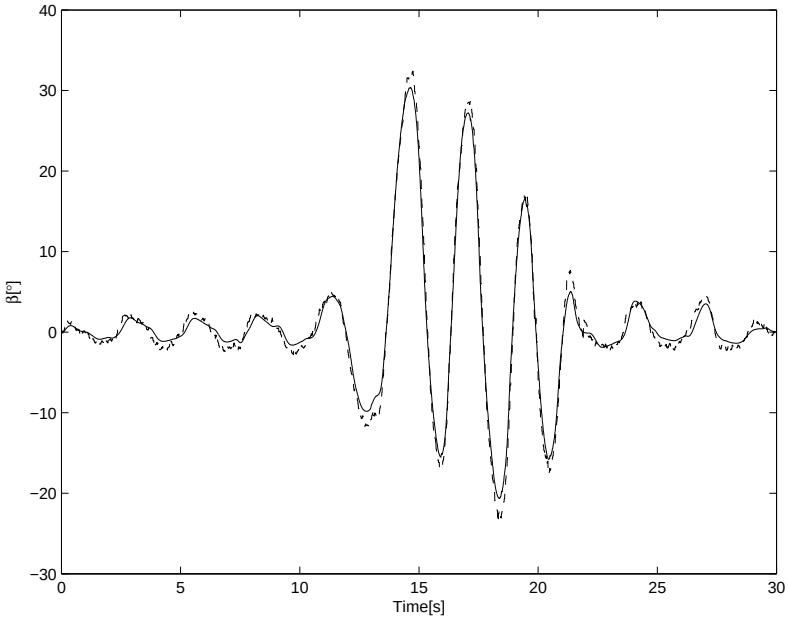

Figure 4.3: Estimate (solid) and measurement (dashed) of vehicle side slip, high friction coefficient.

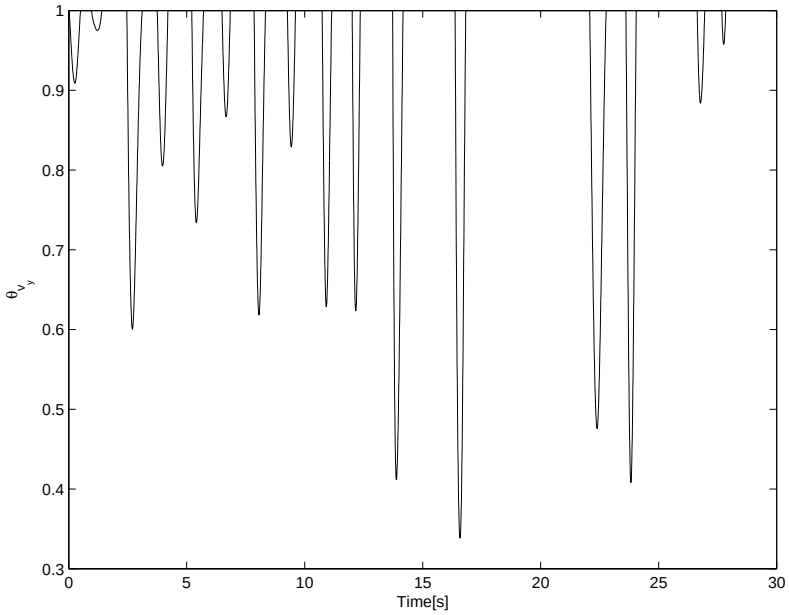

Figure 4.4: Adapted lateral velocity parameter, high friction coefficient.

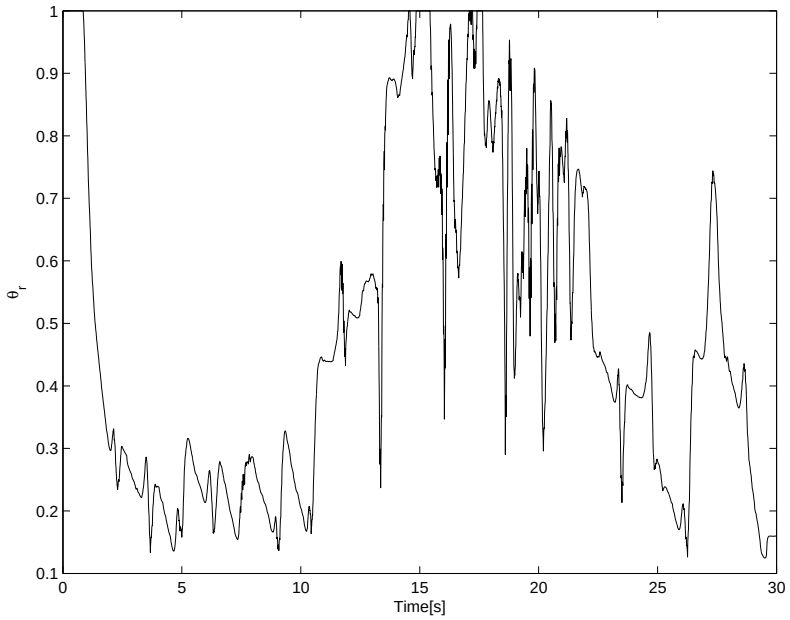

Figure 4.5: Adapted yaw rate parameter, high friction coefficient.

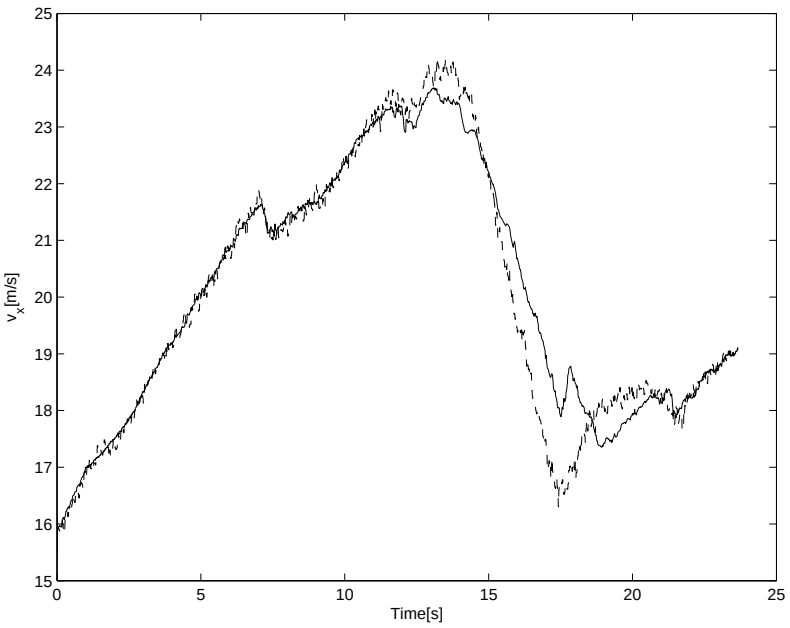

Figure 4.6: Estimate (solid) and measurement (dashed) of longitudinal velocity, low friction coefficient.

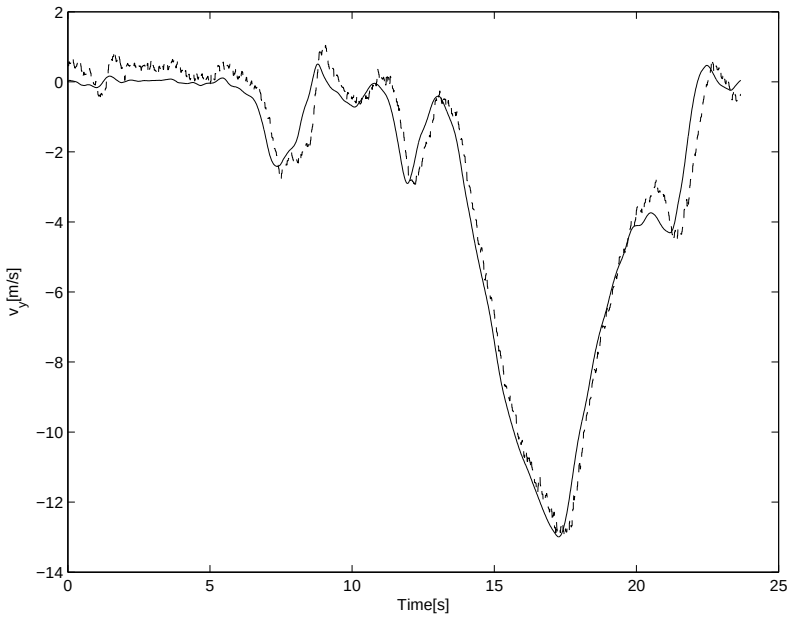

Figure 4.7: Estimate (solid) and measurement (dashed) of lateral velocity, low friction coefficient.

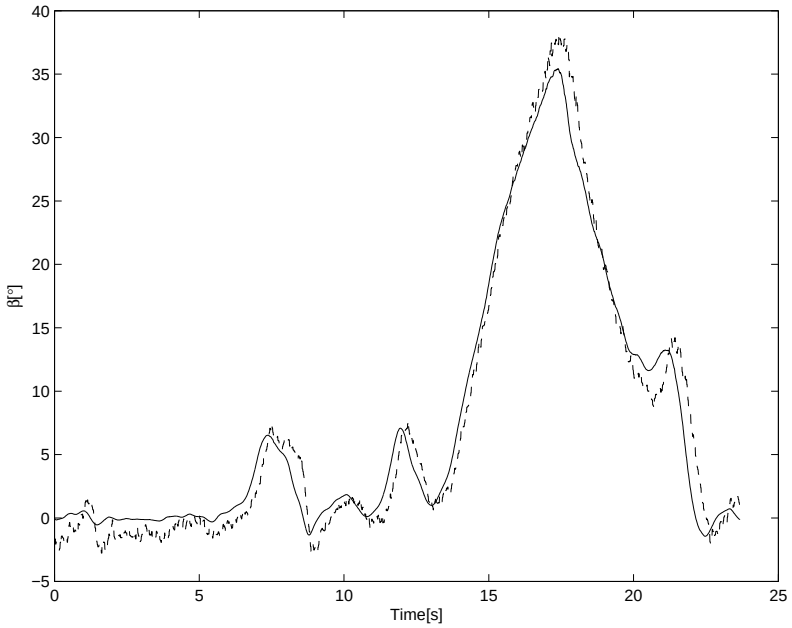

Figure 4.8: Estimate (solid) and measurement (dashed) of vehicle side slip, low friction coefficient.

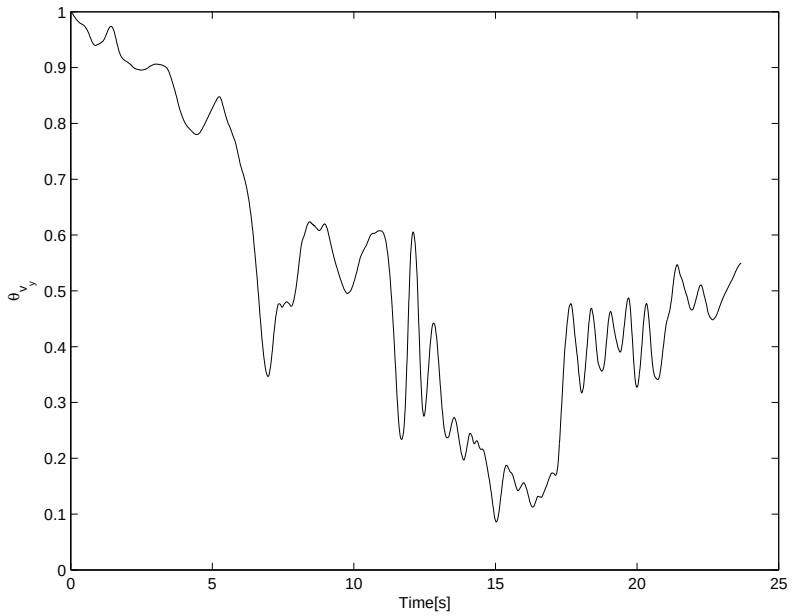

Figure 4.9: Adapted lateral velocity parameter, low friction coefficient.

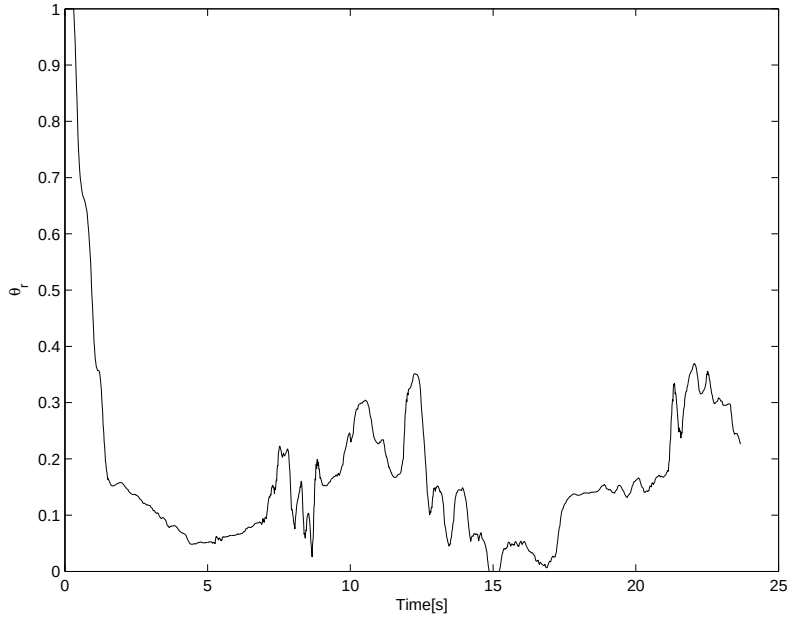

Figure 4.10: Adapted yaw rate parameter, low friction coefficient.

Chapter 5

Preliminary velocity observer design with multiple model friction estimation

5.1 Introduction

The main objective is to augment the nonlinear automotive vehicle velocity observer in [7] with a mechanism for estimation of key friction parameters such as the adhesion coefficient.

5.2 Multiple model friction estimation

The overall idea is illustrated in Figure 5.1, where a number of friction models are evaluated in parallel with the nonlinear velocity observer. The friction models predict the lateral force at each wheel and uses this to predict the lateral acceleration of the vehicle, which is compared to the measured lateral acceleration. The output of each friction model is the lateral acceleration residual, and the multiple friction models differ only in the adhesion coefficient.

The "Filtering and decision logic" block contains the following functions

- High-pass filtering of the residuals in order to avoid interaction between the nonlinear observer and the multiple model friction estimator, since the multiple friction models rely on velocities estimated by the nonlinear observer using the current adhesion coefficient estimate. This is beneficial because the nonlinear observer will attempt to make the residuals with the current adhesion coefficient estimate small, even if this is an incorrect estimate. Hence, there is most information about the friction model errors in frequencies above the nonlinear observer bandwidth.
- Computation of a moving-window average of each residual. This is achieved by taking the absolute value of the residual, and low-pass filtering with a first order filter with bandwidth 0.5 rad/s.

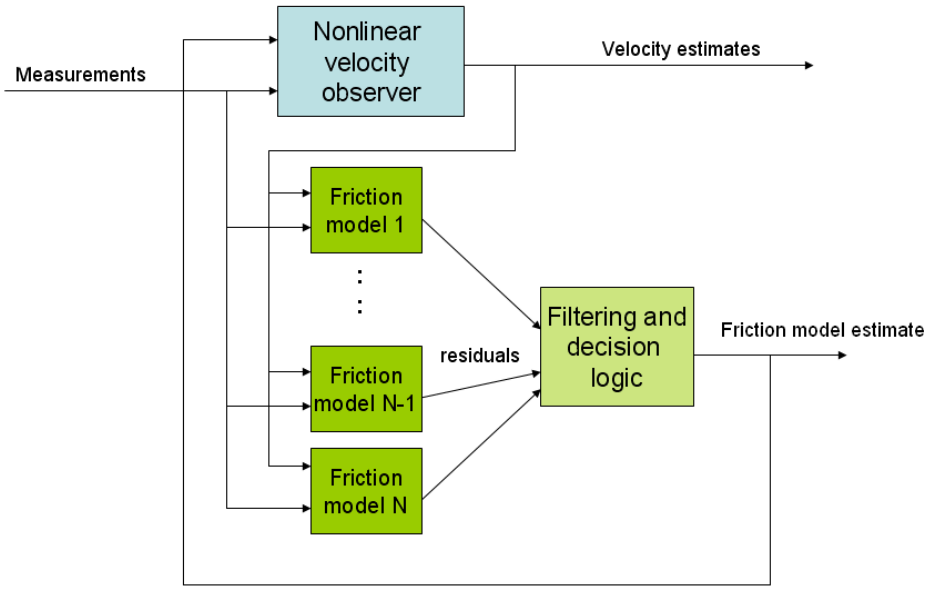

Figure 5.1: Block diagram with state observer using multiple friction models

- The purpose of the decision logic is to compare the friction model residuals resulting from different adhesion coefficients. Based on these residuals it will attempts to select the best estimate among them. In conditions with sufficiently high persistence of excitation, it simply selects the one that gives smallest averaged residual.
- The decision logic monitors persistence of excitation, and will keep the previous adhesion coefficient estimate if there is little excitations. This can be detected if i) all residuals are small, ii) the difference between all the residuals are small, iii) the estimate with smallest residual is not much better than the previous estimate.
- It is experienced that in driving conditions with low persistence of excitation, the velocity observer can have give extremely inaccurate estimates if the adhesion coefficient estimate is too low. On the other hand, an over-estimate tends to give a bias but significantly less errors. To counteract these problems the adhesion coefficient estimate is periodically reset (every 2 seconds) to a high value $\mu_H = 1$, and the associated moving-window filter state is also reset.

The key issue determining the performance of the velocity observer is our ability to detect situations with low persistence of excitation and prevent very large errors in the observer due to too low adhesion coefficient estimate.

5.3 Experimental results

Preliminary experimental results with slalom manoeuvre on dry asphalt are shown in Figures 5.2 - 5.5. Preliminary experimental results on ice are shown in Figures 5.6 - 5.9.

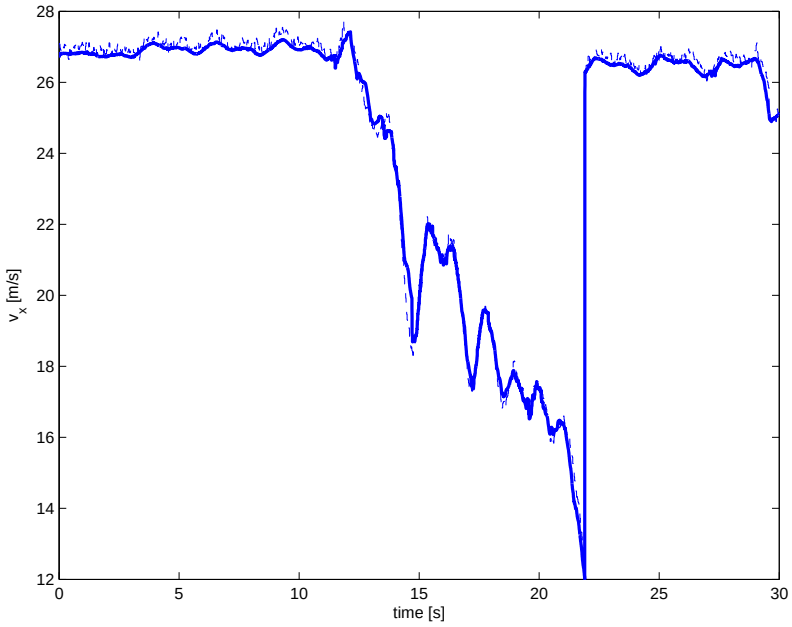

Figure 5.2: Estimate (solid) and measurement (dashed) of longitudinal velocity, slalom manoeuver on dry road, modular observer.

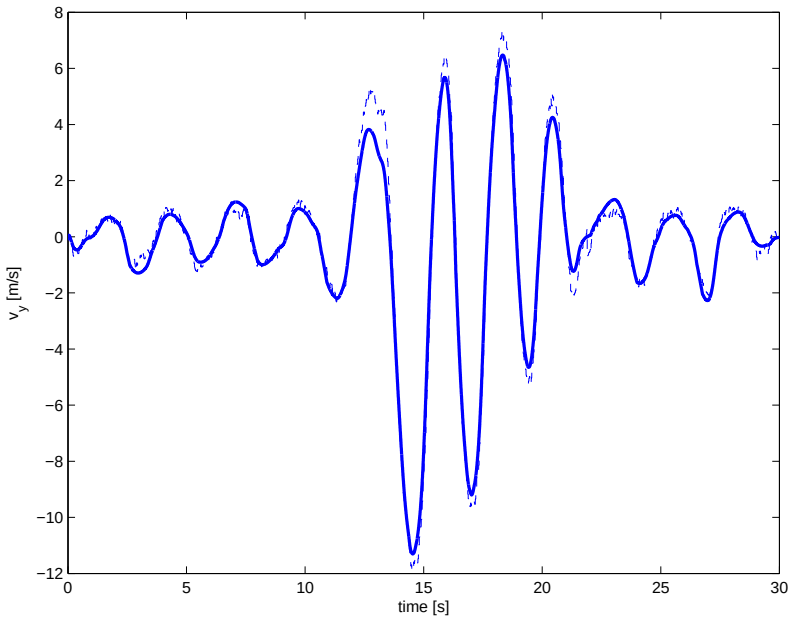

Figure 5.3: Estimate (solid) and measurement (dashed) of lateral velocity, slalom manoeuver on dry road, modular observer.

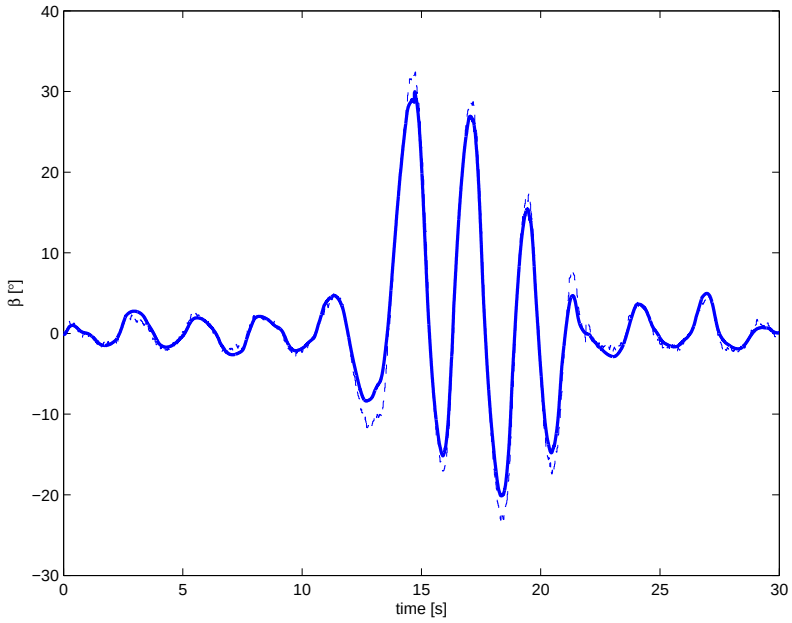

Figure 5.4: Estimate (solid) and measurement (dashed) of side slip, slalom manoeuver on dry road, modular observer.

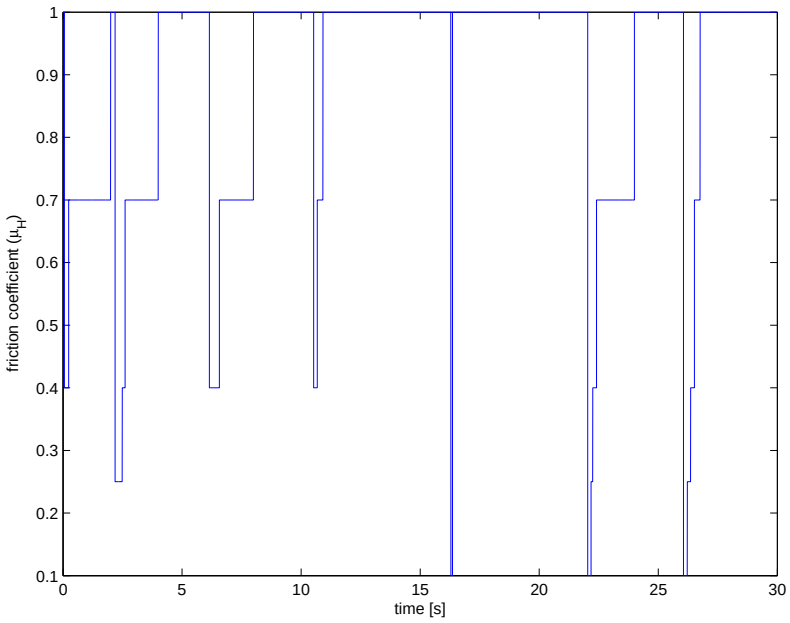

Figure 5.5: Estimate of friction coefficient, slalom manoeuver on dry road, modular observer.

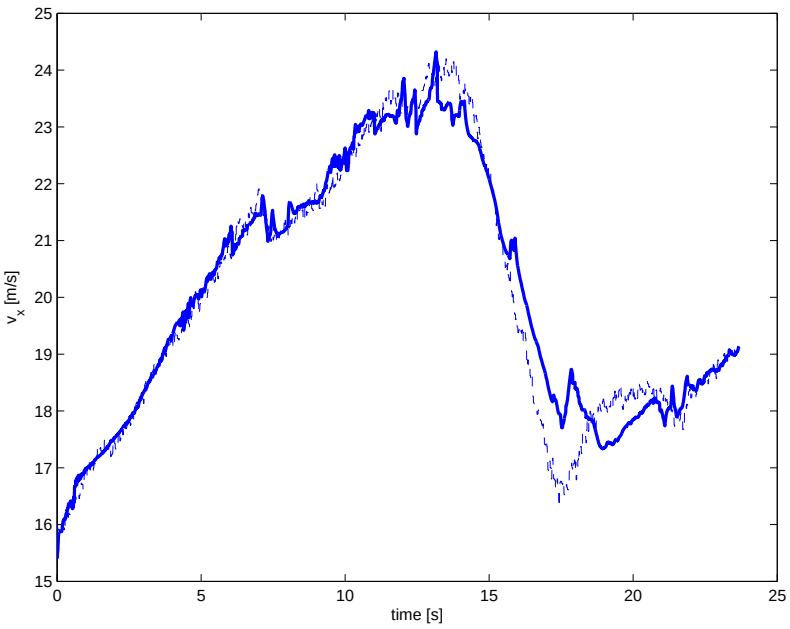

Figure 5.6: Estimate (solid) and measurement (dashed) of longitudinal velocity, circle on ice, modular observer.

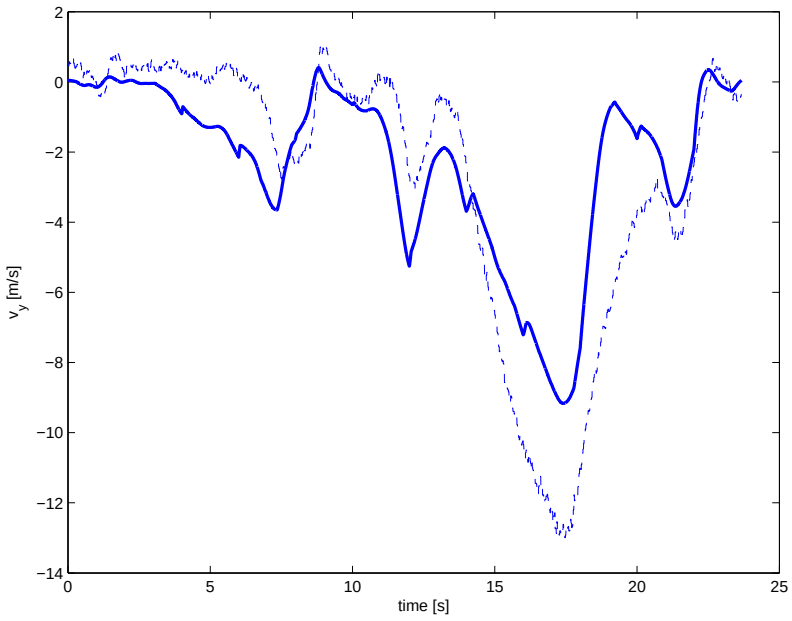

Figure 5.7: Estimate (solid) and measurement (dashed) of lateral velocity, circle on ice, modular observer.

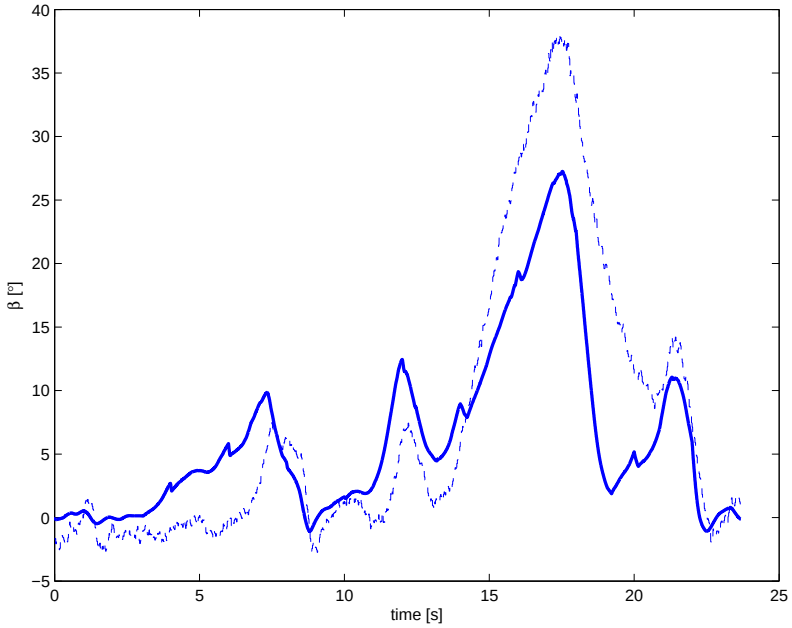

Figure 5.8: Estimate (solid) and measurement (dashed) of side slip, circle on ice, modular observer.

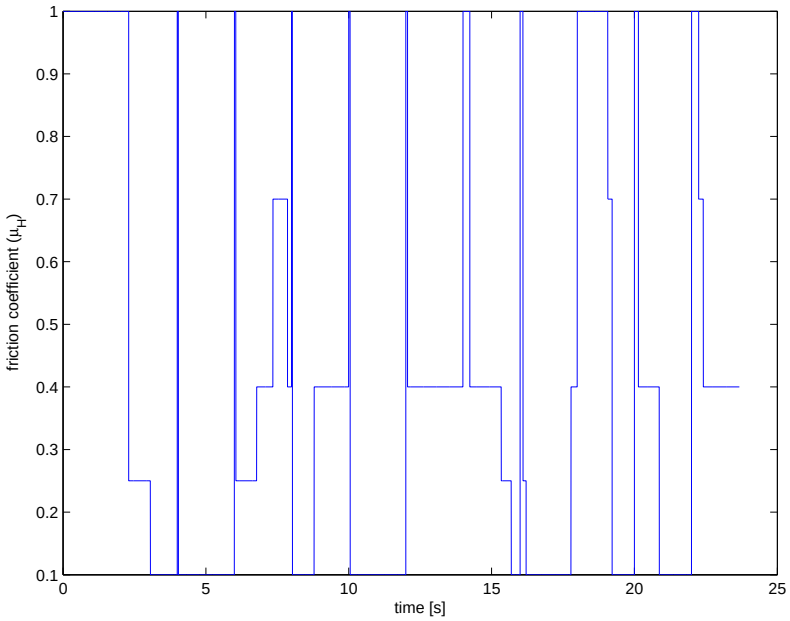

Figure 5.9: Estimate of friction coefficient, circle on ice, modular observer.

Bibliography

[1] M. C. Best, T. J. Gordon, and P. J. Dixon. An extended adaptive Kalman filter for real-time state estimation of vehicle handling dynamics. *Vehicle System Dynamics*, 34:57–75, 2000.

[2] CEMACS. Test vehicle specification. Technical Report D11, 2005.

[3] Jim Farrelly and Peter Wellstead. Estimation of vehicle lateral velocity. In *Proc. 35th IEEE Conf. Decision Contr.*, pages 552–557, 1996.

[4] Yoshiki Fukada. Slip-angle estimation for stability control. *Vehicle Systems Dynamics*, 32:375–388, 1999.

[5] Alexander Hac and Melinda D. Simpson. Estimation of vehicle side slip angle and yaw rate. In *SAE 2000 World Congress*, Detroit, MI, USA, 2000.

[6] Marcus Hiemer, Anne von Vietinghoff, Uwe Kiencke, and Takanori Matsunaga. Determination of vehicle body slip angle with non-linear observer strategies. In *Proceedings of the SAE World Congress*, 2005. Paper no. 2005-01-0400.

[7] L. Imsland, T. A. Johansen, T. I. Fossen, J. Kalkkuhl, and A. Suissa. Vehicle velocity estimation using nonlinear observers. Submitted Automatica, 2005.

[8] Lars Imsland, Tor Arne Johansen, Thor Inge Fossen, Jens Kalkkuhl, and Avshalom Suissa. Vehicle velocity estimation using nonlinear observers. In *Proc. 41th IEEE Conf. Decision Contr.*, 2005. Accepted.

[9] P. A. Ioannou and P. V. Kokotovic. *Adaptive Systems with Reduced Models*. Springer Verlag, New York, NY, 1983.

[10] Jens Kalkkuhl, Tor Arne Johansen, and Jens Ludemann. Nonlinear adaptive backstepping with estimator resetting using multiple observers. In Rolf Johansson and Anders Rantzer, editors, *Nonlinear and Hybrid Systems in Automotive Control*. Springer Verlag, 2003.

[11] Hassan K. Khalil. *Nonlinear Systems*. Prentice Hall, Upper Saddle River, NJ, 3rd edition, 2002.

[12] Uwe Kiencke and Armin Daiss. Observation of lateral vehicle dynamics. *Control Engineering Practice*, 5(8):1145–1150, 1997.

[13] Uwe Kiencke and Lars Nielsen. *Automotive Control Systems*. Springer, 2000.

[14] G. Kresselmeier and K. S. Narendra. Stable model reference adaptive control in the presence of bounded disturbances. *IEEE Transactions on Automatic Control*, 1982.

[15] J. Lu and T. A. Brown. Vehicle side slip angle estimation using dynamic blending and considering vehicle attitude information. Patent US 6671595, 2003.

[16] K. S. Narendra and A. M. Annaswamy. *Stable Adaptive Systems*. Prentice Hall Inc., Boston, MA, 1989.

[17] Hans B. Pacejka. *Tyre and vehicle dynamics*. Butterworth-Heinemann, 2002.

[18] B. B. Peterson and K. S. Narendra. Bounded error adaptive control. *IEEE Transactions of Automatic Control*, 1982.

[19] Laura R. Ray. Nonlinear state and tire force estimation for advanced vehicle control. *IEEE Transactions on Control Systems Technology*, 3(1):117–124, 1995.

[20] Laura R. Ray. Nonlinear tire force estimation and road friction identification: simulation and experiments. *Automatica*, 33(10):1819–1833, 1997.

[21] Eduardo D. Sontag and Yuan Wang. On characterizations of the input-to-state stability property. *Systems Control Lett.*, 24(5):351–359, 1995.

[22] A. Suissa, Z. Zomotor, and F. Böttiger. Method for determining variables characterizing vehicle handling. Patent US 5557520, 1996.

[23] Ali Y. Ungoren and Huei Peng. A study on lateral speed estimation methods. *Int. J. Vehicle Autonomous Systems*, 2(1/2):126–144, 2004.

[24] Anton T. van Zanten. Bosch ESP system: 5 years of experience. In *In Proceedings of the Automotive Dynamics & Stability Conference (P-354)*, 2000. Paper no. 2000-01-1633.

[25] Paul J. Th. Venhovens and Karn Nab. Vehicle dynamics estimation using Kalman filters. *Vehicle System Dynamics*, 32:171–184, 1999.